International Journal of Nanomedicine

Dovepress
Taylor & Francis Group

Open Access Full Text Article

ORIGINAL RESEARCH

A Novel Integrated Approach: Plant-Mediated Synthesis, in vitro and in silico Evaluation of Silver Nanoparticles for Breast Cancer and Bacterial Therapies

Sahar S Alghamdi[1–3], Haifa A Alhaidal[1], Afrah E Mohammed[4,5], Arwa Alsubait[2,6], Maali D Alshammari[7], Lamis Alsaqer[1], Shahad Saleem Alzahrani[1], Fai Alanazi[1], Layan Basel Al Tuhayni[1], Rizwan Ali[2], Shaden Alharbi[1], Bader Hazazi[2], Mona E AlEnazi[8], Zeyad I Alehaideb[2]

[1]College of Pharmacy (COP), King Saud bin Abdulaziz University for Health Sciences (KSAU-HS), Riyadh, Saudi Arabia; [2]Medical Research Core Facility and Platforms, King Abdullah International Medical Research Center (KAIMRC), Ministry of National Guard - Health Affairs, Riyadh, Saudi Arabia; [3]King Abdulaziz Medical City, Ministry of the National Guard - Health Affairs, Riyadh, 11426, Saudi Arabia; [4]Department of Biology, College of Science, Princess Nourah bint Abdulrahman University (PNU), Riyadh, 11671, Saudi Arabia; [5]Microbiology and Immunology Unit, Natural and Health Sciences Research Center, Princess Nourah bint Abdulrahman University, Riyadh, Saudi Arabia; [6]Department of Clinical Laboratory Sciences, College of Applied Medical Sciences, King Saud bin Abdulaziz University for Health Sciences, Riyadh, Saudi Arabia; [7]Department of Pharmaceutical Chemistry, College of Pharmacy, University of Hail, Hail, Saudi Arabia; [8]Department of Zoology, College of Science, King Saud University, Riyadh, Saudi Arabia

Correspondence: Sahar S Alghamdi, Associate Professor, Department of Pharmaceutical Sciences at King Saud bin Abdulaziz University for Health Sciences (KSAU-HS), Riyadh, Saudi Arabia, Email Ghamdisa@ksau-hs.edu.sa

Video Abstract

Point your SmartPhone at the code above. If you have a QR code reader the video abstract will appear. Or use: https://youtu.be/DXHCrQ8yitc.

Background and Aim: Nanotechnology offers a promising approach to address breast cancer and bacterial resistance, two critical global health challenges. This study synthesized silver nanoparticles (AgNPs) using extracts from *Rhazya stricta* (*R.S*). *Calotropis procera* (*C.P*). and *Calligonum comosum* (*C.C*) to evaluate their potential as novel therapeutic agents.

Materials and Methods: AgNP synthesis was achieved via co-precipitation, and their characterization was performed using various techniques. Cytotoxicity was assessed using the MTT assay against multiple breast cancer cell lines (KAIMRC2, MDA-MB231, MCF-7) and a non-malignant control (MCF-10A). Antimicrobial activity was evaluated using a well diffusion assay against *Staphylococcus aureus* and *Escherichia coli*. LC-MS identified several bioactive metabolites, which were further analyzed in silico computational analysis to predict their anti-cancer and antibacterial properties.

Results: The resulting AgNPs demonstrated significant cytotoxicity against breast cancer cells with minimal toxicity to normal cells, and potent antibacterial activity. Specifically, *R.S*.-AgNPs showed strongest activity against MDA-MB-231, *C.P*.-AgNPs against MCF-7, and *C.C*.-AgNPs against KAIMRC-2. Promising lead metabolites, including 1-Acetylaspidospermidine, Apigenin-7-o-glucoside, and Chlorogenic acid, were identified, suggesting potential for development as novel oral anti-cancer and antibacterial agents.

Conclusion: Further research focusing on the optimization and preclinical development of these identified metabolites is warranted to explore their translational potential as oral anti-cancer and antibacterial agents.

Keywords: nanomedicine, anti-cancer, bactericidal, *Rhazya stricta*, *Calotropis procera*, *Calligonum comosum*

Introduction

Breast cancer is one of the most frequently diagnosed tumors worldwide and is a leading cause of death among women.[1] The classification of breast cancer is based on its genetic and hormone characteristics, such as the expression of the estrogen receptor (ER), progesterone receptor (PR), and human epidermal growth factor receptor 2 (HER2), providing a framework for diagnosis, management, and prognostic evaluation. The absence of these receptors characterizes the most

Received: 3 February 2025
Accepted: 13 May 2025
Published: 19 August 2025

aggressive form of breast cancer, known as triple-negative breast cancer (TNBC).[2] Despite the availability of various anti-cancer agents, the development of chemoresistance and undesirable side effects limit their therapeutic benefits.[3] Hence, the discovery of novel, highly effective treatments for breast cancer is urgently required.

Nanocarrier drug delivery systems based on nanomedicine have the potential to overcome the limitations of conventional drug delivery methods, including low bioavailability, non-specific biodistribution, and low therapeutic indices.[4] These nanocarriers, derived from various molecular compositions, offer precise and controlled delivery of therapeutic drugs and other ligands, addressing the limitations of conventional drug delivery methods.

Numerous studies have highlighted the potential of herbs as mediators in the synthesis of metal nanoparticles (NPs).[5–8] Various medicinal herbs, such as *Coriandrum sativum, Mangifera indica, Ocimum sanctum*, and *Bridelia retusa*, have been successfully used to synthesize metal NPs.[9–11] Additionally, plants such as *Eucalyptus sp*. and *Aloe vera* have been incorporated in numerous studies.[9,12–15]

Building on this foundation, *Rhazya stricta* (*R.S).*, *Calotropis procera* (*C.P)*., and *Calligonum comosum* (*C.C)* are widely distributed plant species in the Middle Eastern region. These plants play a vital role in traditional medicine, treating various diseases, including cancer and bacterial infections.[5–7] Several studies have demonstrated that *R.S., C.P.*, and *C.C*. exhibit potent anti-cancer activity, making them promising candidates for the development of new cancer therapies.[3,16–20]

Our recent investigations have examined the anti-proliferative activity of *R.S., C.P.*, and *C.C*. extracts against different cancer cells,[21] this study evaluated several cancer cell lines including MCF-7 (ER and PR-positive breast cancer cell line from a Caucasian patient), MDA-MB-231 (TNBC cell line from a Caucasian patient), and KAIMRC-2 (TNBC cell line from a Saudi patient) in vitro. Based on our previous work, we hypothesized that *R.S., C.P.*, and *C.C*. would exhibit superior biological activity against cancer and bacterial infections if the plant extracts were encapsulated into silver nanoparticles. Multiple characterization methods were applied to evaluate the formulated nanoparticles, followed by in vitro biological evaluation against multiple breast cancer cell lines and bacterial strains. Additionally, to identify the secondary metabolites present in the extract, liquid chromatography-mass spectrometry (LC-MS) was utilized, followed by thorough in silico investigations to explore the pharmacodynamics and pharmacokinetics properties of the metabolites, aiming to find potential leads for further research and development.

Although the green synthesis of AgNPs using plant extracts has been extensively investigated, this study advances the field by examining novel plant sources that have not yet been explored for AgNPs synthesis. The distinct phytochemical profiles of these plants offer new insights into their influence on NP formation and associated biological activities.

Moreover, despite the routine application of established characterization techniques, their use remains fundamental in validating the successful synthesis and stability of the NPs, thereby ensuring consistency and reproducibility in future research and applications.

Materials and Methods

Plant Material Preparation and Extraction

Aerial parts of *R.S., C.P.*, and *C.C*. were obtained from a local market in Saudi Arabia. The plant materials were authenticated by a botanical expert, Professor Mona Alwhibi, at King Saud University and assigned the accession number 24321 for *R.S*., 24317 for *C.P*., and 24328 for *C.C*. The authenticated plant materials were thoroughly washed with distilled water to remove any dirt or contaminants, then air-dried at room temperature (25 ± 2°C) for 7 days.

The dried plant materials were ground into a fine powder using an electronic grinder with a mesh size of 0.5 mm. The powdered materials (100 g each) were subjected to Soxhlet extraction using analytical grade methanol (1 L) as the solvent. The extraction process was carried out for 48 hours at a controlled temperature of 40 ± 1°C using a temperature-controlled water bath.

After extraction, the methanolic extracts were filtered through Whatman No. 1 filter paper to remove any particulate matter. The filtered extracts were then concentrated using a rotary evaporator (Buchi R-210, Switzerland) at 40°C under reduced pressure (175 mbar). The resulting concentrated extracts were transferred to pre-weighed glass vials and further dried in a vacuum desiccator for 24 hours to remove any residual solvent. The dried extracts were stored in airtight containers at 4°C until further use.

Biosynthesis of Silver Nanoparticles (AgNPs)

Preparation of Plant Extracts

Aqueous extracts of *R.S., C.P.*, and *C.C.* were prepared by mixing 2 g of each powdered plant material with 100 mL of double-distilled water (2% w/v) in separate 250 mL Erlenmeyer flasks. The mixtures were heated at 90 ± 2°C for 15 minutes using a temperature-controlled water bath with constant stirring at 200 rpm. After cooling to room temperature, the extracts were filtered through Whatman No. 1 filter paper (pore size: 11 μm) to remove any plant debris. The filtered extracts were stored at 4°C and used within 24 hours to ensure freshness.

Synthesis of AgNPs

For the biosynthesis of AgNPs, 10 mL of each prepared plant extract was added individually to 90 mL of 1 mM silver nitrate ($AgNO_3$) solution in separate 250 mL Erlenmeyer flasks. The $AgNO_3$ solution was prepared using analytical grade $AgNO_3$ (Sigma-Aldrich, USA) dissolved in double-distilled water. The mixtures were heated at 90 ± 2°C for 30 minutes with constant stirring at 150 rpm using a magnetic stirrer hot plate.

After heating, the reaction mixtures were cooled to room temperature and covered with aluminum foil to be protected from light. The solutions were then incubated at room temperature (25 ± 2°C) under dark conditions for 24 hours until the color had been changed.

Purification of AgNPs

The synthesized AgNPs were purified using a two-step centrifugation process. First, the solutions were centrifuged at 4700 rpm for 10 minutes using a refrigerated centrifuge at 4°C. The supernatant was carefully discarded, and the pellet was resuspended in 10 mL of double-distilled water. This suspension was then subjected to a second centrifugation step at 13400 rpm for 5 minutes.

The resulting pellet was washed twice with 10 mL of double-distilled water to remove any unbound plant extracts or unreacted silver ions. After the final wash, the purified AgNPs were dried at room temperature for 24 hours in a laminar flow hood. The dried AgNPs were weighed, and stock solutions of 1 mg/mL concentration were prepared from each plant-mediated AgNP by resuspending in sterile double-distilled water. These stock solutions were stored at 4°C in amber glass vials for further characterization and biological activity studies.

Characterization of AgNPs

Transmission Electron Microscopy (TEM)

The morphology and size distribution of the synthesized AgNPs were examined using a JEM-1011 transmission electron microscope (JEOL, Japan) operated at an accelerating voltage of 80 kV. Sample preparation involved placing a drop (10 μL) of the purified AgNP suspension onto a carbon-coated copper grid (200 mesh, Ted Pella, USA). Excess liquid was removed using filter paper, and the grid was allowed to dry in a vacuum desiccator for 2 hours before analysis. Multiple fields of view were captured for each sample to ensure representative imaging. The size distribution of the AgNPs was determined by measuring their diameter using ImageJ software (NIH, USA).[20]

Dynamic Light Scattering (DLS) and Zeta Potential Measurement

The hydrodynamic size distribution and zeta potential of the AgNPs were determined using a Zetasizer Nano ZS (Malvern Panalytical Ltd, UK). For DLS measurements, 1 mL of each AgNP suspension (0.1 mg/mL in double-distilled water) was placed in a disposable polystyrene cuvette. The measurements were performed at 25°C with a scattering angle of 173°. For zeta potential measurements, the same suspensions were transferred to a folded capillary zeta cell. All measurements were performed in triplicate, with each measurement consisting of 15 runs. The data were analyzed using the Zetasizer software (version 7.13) to obtain the average hydrodynamic diameter, polydispersity index (PDI), and zeta potential values.[21]

Elemental Analysis

The elemental composition of the synthesized AgNPs was analyzed using energy-dispersive X-ray spectroscopy (EDS) coupled with scanning electron microscopy (SEM). A Jeol (JED-2200 series, Tokyo, Japan) SEM-EDS system was used

for this analysis. Samples were prepared by drop-casting 10 μL of AgNP suspension onto a silicon wafer and allowing it to dry under ambient conditions. The samples were then sputter-coated with a thin layer of gold (approximately 5 nm) to enhance conductivity. EDS spectra were collected at an accelerating voltage of 15 kV, with a working distance of 10 mm and a collection time of 100 seconds per spectrum. At least three different areas were analyzed for each sample to ensure representative results.

Fourier-Transform Infrared Spectroscopy (FTIR)

FTIR analysis was conducted to identify the potential plant metabolites involved in the reduction and stabilization of AgNPs. A SPECTRUM100 FTIR spectrometer (Perkin-Elmer, Wellesley, MA, USA) equipped with an attenuated total reflectance (ATR) accessory was used for this analysis. Samples were prepared by mixing 1 mg of dried AgNPs with 100 mg of spectroscopic grade KBr and pressing the mixture into a pellet using a hydraulic press. FTIR spectra were recorded in the range of 4000–400 cm^{-1} with a resolution of 4 cm^{-1} and 32 scans per sample. Background correction was performed using a blank KBr pellet. The obtained spectra were analyzed using OPUS software (version 7.5, Bruker) to identify characteristic peaks and functional groups.

Biological Activity Assays

Anticancer Activity

Cell Culture

Human breast cancer cell lines (MDA-MB231, MCF-7) and a non-tumorigenic epithelial cell line (MCF-10A) were obtained from the American Type Culture Collection (ATCC, USA). Moreover, a breast cancer cell line (KAIMRC2), which was isolated and characterized at King Abdullah International Medical Research Center in Riyadh, Saudi Arabia, as previously described and documented[20] was evaluated in the study. The cells were maintained in Advanced Dulbecco's Modified Eagle Medium (DMEM) supplemented with 10% heat-inactivated fetal bovine serum (FBS), 2 mM L-glutamine, 100 U/mL penicillin, and 100 μg/mL streptomycin (all from Gibco, USA). Cells were cultured in a humidified incubator at 37°C with 5% CO_2 atmosphere. The culture medium was changed every 2–3 days, and cells were passaged using 0.25% trypsin-EDTA solution when they reached 80–90% confluence.

Cell Viability Assay

The cytotoxic effects of the synthesized AgNPs were evaluated using the 3-(4,5-dimethylthiazol-2-yl)-2,5-diphenyltetrazolium bromide (MTT) assay.[22] Cells were seeded in 96-well plates at a density of 1×10^4 cells per well in 100 μL of complete growth medium. After 24 hours of incubation to allow cell attachment, the medium was replaced with a fresh medium containing various concentrations of AgNPs (0, 6.25, 12.5, 25, 50, 100, 200, 400, and 600 μg/mL). Each concentration was tested in triplicate.

After 48 hours of treatment, 10 μL of MTT solution (5 mg/mL in PBS) was added to each well, and the plates were incubated for an additional 3 hours at 37°C. The medium was then carefully aspirated, and 100 μL of DMSO was added to each well to dissolve the formazan crystals. The plates were gently shaken for 10 minutes to ensure complete dissolution. The absorbance was measured at 570 nm using a Spectramax M3 microplate reader (Molecular Devices, USA). Cell viability was calculated as a percentage relative to untreated control cells. Mitoxantrone (Sigma-Aldrich, USA) was used as a positive control at concentrations ranging from 0.01 to 10 μM.

Antibacterial Activity

Bacterial Strains and Culture Conditions

The antibacterial activity of the synthesized AgNPs was evaluated against two pathogenic bacterial strains: *Staphylococcus aureus* (*S. aureus*) ATCC 25923 (gram-positive) and *Escherichia coli* (*E. coli*) ATCC 25922 (gram-negative). The bacterial strains were obtained from the Bio-house medical lab in Riyadh, Saudi Arabia. The strains were maintained on nutrient agar slants at 4°C and subcultured on fresh nutrient agar plates 24 hours before the experiments.

Preparation of Bacterial Suspensions

Bacterial suspensions were prepared using the direct colony suspension method. Several colonies from a 24-hour culture

on nutrient agar were suspended in sterile 0.9% saline solution. The turbidity of the suspension was adjusted to match the 0.5 McFarland standard, corresponding to approximately 1.5×10^8 CFU/mL. This suspension was then diluted 1:10 in sterile saline to obtain a working suspension of approximately 1.5×10^7 CFU/mL for use in the agar well diffusion assay.

Agar Well Diffusion Assay

The antibacterial activity of the AgNPs was determined using the agar well diffusion method. Mueller-Hinton agar plates were prepared according to the manufacturer's instructions and allowed to solidify. The working bacterial suspensions (100 µL) were spread evenly on the agar surface using a sterile cotton swab. Three wells (6 mm in diameter) were punched in the agar using a sterile cork borer.

AgNP suspensions (50 µL) at concentrations of 1 mg/mL were added to each well. Sterile distilled water was used as a negative control, and Ampicillin (10 µg/mL) served as a positive control. The plates were incubated at 37°C for 24 hours. After incubation, the diameter of the inhibition zone around each well was measured using a digital caliper. The experiments were performed in triplicate.

Data Analysis

The half-maximal inhibitory concentration (IC_{50}) values were determined using GraphPad Prism software (version 10, GraphPad Software Inc., USA). Dose-response curves were generated using non-linear regression analysis, and IC_{50} values were calculated from these curves. All experiments were performed in triplicate and repeated three times independently. The antibacterial activity was expressed as the mean diameter of the inhibition zone (mm) ± standard deviation. Statistical analysis was performed using one-way ANOVA followed by Tukey's post-hoc test to compare the effectiveness of different AgNP concentrations and plant sources. A p-value < 0.05 was considered statistically significant.

Liquid Chromatography Quadrupole Time-of-Flight Mass Spectrometry (LC-QTOF-MS) Analysis

Sample Preparation

Aqueous extracts of *R.S., C.P.*, and *C.C.* were prepared by mixing 1 g of dried plant powder with 100 mL of double-distilled water. The mixtures were heated at 60°C for 48 hours with constant stirring at 150 rpm. After cooling, the extracts were filtered through Whatman No. 1 filter paper and concentrated using a rotary evaporator. The concentrated extracts were then lyophilized to obtain dry powders.

For LC-MS analysis, 1 mg of each lyophilized extract was dissolved in 1 mL of either HPLC-grade methanol or water containing 0.1% formic acid. The solutions were vortexed for 1 minute and centrifuged at 13,000 rpm for 10 minutes to remove any insoluble particles. The supernatants were filtered through 0.22 µm PTFE syringe filters before injection into the LC-MS system.

LC-QTOF-MS Analysis

The LC-QTOF-MS analysis was performed using an Agilent 1290 Infinity II UHPLC system coupled to an Agilent 6545 Q-TOF mass spectrometer (Agilent Technologies, USA). Chromatographic separation was achieved on an Agilent ZORBAX Eclipse Plus C18 column (2.1 × 100 mm, 1.8 µm particle size) maintained at 40°C. The mobile phase consisted of (A) water with 0.1% formic acid and (B) acetonitrile with 0.1% formic acid. The gradient elution program was as follows: 0–1 min, 5% B; 1–15 min, 5–95% B; 15–20 min, 95% B; 20–21 min, 95–5% B; 21–25 min, 5% B. The flow rate was set at 0.3 mL/min, and the injection volume was 2 µL. The Q-TOF mass spectrometer was operated in both positive and negative ionization modes using an electrospray ionization (ESI) source. The MS parameters were set as follows: capillary voltage, 3500 V; nozzle voltage, 1000 V; fragmentor voltage, 175 V; skimmer voltage, 65 V; drying gas temperature, 250.

In Silico Studies

Prediction of Bioactivity Using PASS Online Web Server

The Prediction of Activity Spectra for Substances software (PASS; http://way2drug.com/PassOnline/, accessed on 16 March 2023) was utilized to assess the bioactivities of the metabolites, including anticancer and antimicrobial activities.[22] This software has an accuracy of approximately 85% in predicting more than 4000 types of pharmacological and toxicological activities, depending on the submitted compound structures, which were subsequently screened using a structure-activity relationship database. Each predicted target in the PASS is represented by two values: P_a and P_i, where P_a represents the probability of the metabolite interacting with a respective target, and P_i represents the probability that it does not interact. A P_a value greater than 0.3 indicates less plausible potential for the predicted activity, whereas a P_a value greater than 0.5 suggests a relatively high probability. Moreover, a P_a value greater than 0.7 indicates a high likelihood that the study has demonstrated the possible metabolite. Nevertheless, it is important to note that experimental studies are necessary to validate the predictions made by PASS, other factors can influence biological activity.

Predictions of Absorption, Distribution, Metabolism, and Excretion (ADME) Properties

The SMILES (Simplified Molecular Input Line Entry System) codes for each compounds were obtained and applied to the calculations using the SwissADME (http://www.swissadme.ch/, accessed on 16 March 2023).[23] It allows the analysis of physicochemical descriptors and estimation of ADME parameters, pharmacokinetic properties, drug-like properties, and medicinal chemistry properties for the bioactive molecules identified in *R.S., C.P.*, and *C.C.*[23]

Cytochromes P450 (CYP450) Enzymes Inhibition Profile

Five crucial CYP450 enzymes including CYP1A2, CYP2C19, CYP2C9, CYP2D6, and CYP3A4 were evaluated using SwissADME webserver to perceive the effect of these aerials on these important enzymes, and SMILES was used as input.

Prediction of Organ and Endpoint Toxicity Analysis Using ProTox II

Protox-II (https://tox-new.charite.de/protox_II/, accessed on 16 March 2023) is an in silico toxicity model that estimates the potential toxicity of chemicals affecting humans, animals, or plants. It aims to minimize the cost and need for animal trails since it provides a prediction for the intensity of toxicity.[24] The interpretation of results has been largely established by rich-information data sources such as DSSTox (Distributed Structure- Searchable Toxicity) and CEBS: a comprehensively annotated database of toxicological data. In our study, the Protox-II webserver was utilized to explore the subsurface of the characteristic of identified metabolites in terms of toxicity, represented in lethal dose (LD_{50}), organ toxicity, and toxicity endpoints. Five different sections were established in the Protox-II webserver to measure toxicity: (1) acute toxicity (oral toxicity model with six different toxicity classes); (2) organ toxicity (one model); (3) toxicological endpoints (four models); (4) toxicological pathways (12 models) and (5) toxicity targets (15 models). Herein, we mainly focused only on the first three classes. In the first section, the web server determines metabolite toxicity classes based on the estimated lethal dose for each compound after using the SMILES of it and running toxicity prediction. Class one exhibits the most fetal metabolite with an estimated LD_{50} of ≤ 5, on contrary, class 6 was proposed to be the safest with an estimated lethal dose of $LD_{50} > 5000$. For the prediction of organ toxicity, hepatotoxicity is evaluated. Furthermore, toxicological endpoints are demonstrated in four main modules: carcinogenicity, immunogenicity, mutagenicity, and cytotoxicity.

Prediction of Cardiotoxicity Using Pred-hERG 4.2 Online Web Server

The metabolites cardiotoxicity effect was measured using Pred-hERG 4.2 web server (http://predherg.labmol.com.br, accessed on 13 April 2023) since blockage of human ether-à-go-go related gene (hERG) potassium channels can lead to lethal cardiac arrhythmia and toxicity.[25] Web server results allow the differentiation of cardiotoxic from non-cardiotoxic with a confidence level. Moreover, the probability map is used to represent toxicity. The green color represents cardiotoxicity (the darker the color, the more toxic), while pink represents non-cardiotoxicity.

Target Predictions

Molinspiration is a web-based application (https://www.molinspiration.com, accessed on 15 April 2023) used to estimate the bioactivity score of synthetic compounds when tested against typical human receptors such GPCRs, ion channels, kinases, and nuclear receptors, proteases, and enzymes. Score values reveal how likely a molecule has the potential to be a therapeutic candidate.[26] A compound is more likely to have significant biological activities if its bioactivity score exceeds 0.00. In contrast, values between - 0.50 and 0.00 are predicted to be moderately active, and less than - 0.50 is assumed to be inactive.[14] Molinspiration focuses on specific pharmacological classes and the creation of individual activity scores for each of these classes. The screening process in Molinspiration is based on the discovery of pieces or aspects of the substructure that are typical of the active compounds. The collection of active molecules (encoded as SMILES) is adequate for training and does not require knowledge of the receptor's 3D structure. Therefore, the approach may be used even in the early stages of a project when a comprehensive understanding of the binding mode is not yet available.[26]

Swiss target prediction (http://www.swisstargetprediction.ch/, accessed on 14 April 2023) offers an accessible design framework to predict small molecule protein targets. The javascript-based molecular editor of ChemAxon allows users to draw query molecules in 2D. The validity of the SMILES is first verified by comparison to a known chemical structure. If this is true, the similarity (both 2D and 3D) between the query molecule and all ligands in the database is computed. The score of each target is then determined by adding the 2D and 3D similarity values with the ligands that share the greatest similarities.[23,27,28]

Results

Biogenic Synthesis of AgNPs

The present study aimed to evaluate the potential benefits of using *R.S., C.P.*, and *C.C.* aqueous aerial extracts as bio-mediators in the synthesis of AgNPs and to assess their anticancer and antibacterial activities. The plant extracts were introduced into an $AgNO_3$ solution, resulting in a mixture that exhibited a color change from pale yellow to dark brown, indicating the formation of AgNPs. *R.S.* and *C.C.* took only 30 minutes to develop a brown color, whereas *C.P.* took 1 hour. The color intensity increased progressively during the residual reaction time.

AgNPs Characterization

Morphology and Size Distribution

TEM technique was employed to characterize the *R.S., C.P.*, and *C.C.*- AgNPs. TEM images revealed that *R.S.*-AgNPs were evenly dispersed and predominantly spherical, with an average size of 78.87 nm (Figure 1A). *C.P.*-AgNPs displayed an average size of 13.5 nm (Figure 1B), while *C.C.*-AgNPs demonstrated a triangular shape with an average size of 46.95 nm (Figure 1C). Interestingly, despite the triangular shape of *C.C.*-AgNPs, which theoretically could result in decreased biological activity, these nanoparticles exhibited remarkable biological activity.

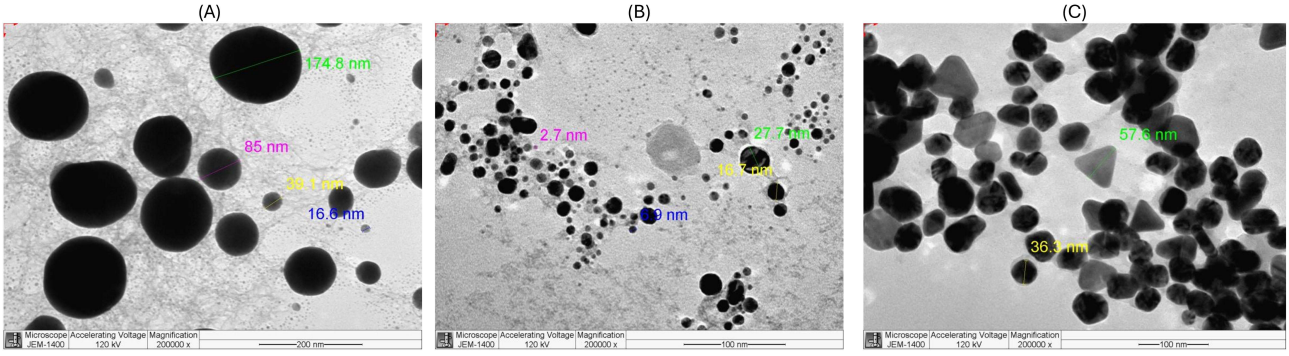

Figure 1 TEM analysis of the synthesized *R.S., C.P.*, and *C.C*-AgNPs. The TEM images revealed that the *R.S., C.P.*, and *C.C*-AgNPs were found in spherical shape and well distributed with an average size of 78.87 nm for *R.S.*-AgNPs (**A**), 13.5 nm for *C.P.*-AgNPs (**B**), and 46.95 nm for *C.C.*-AgNPs (**C**). (N=3).

https://doi.org/10.2147/IJN.S516723

Determination of Particle Size Distribution Using Dynamic Light Scattering (DLS) with a Zetasizer

The zeta size and potential measurements for *R.S.*-AgNPs revealed an average diameter of 44.54 nm and a zeta potential of −8.95 mV. In contrast, *C.P.*-AgNPs exhibited an average diameter of 18.95 nm and a zeta potential of −17.8 mV. Zeta size and potential measurements for *C.C.*-AgNPs, showing an average diameter of 55.05 nm and a zeta potential of −18.1 mV.

Elemental Composition and Surface Morphology

The elemental compositions and surface morphology of the *R.S., C.P.*, and *C.C.*-AgNPs were studied using EDS and SEM, respectively. Figure 2 illustrated the results for *R.S.*-AgNPs, where SEM microphotograph (Figure 2A) showed non-aggregated and spherical shape. EDS analysis (Figure 2B) revealed distinct peaks corresponding to carbon (C), oxygen (O), and silver (Ag). The presence of Ag confirmed the formation of AgNPs, while the other elements indicated successful capping by carbon-based phytochemicals and plant metabolites. Furthermore, the percentage relative composition of the elements is displayed in (Figure 2C). Similarly, Figure 3 summarized the findings for *C.P.*-AgNPs, with Figure 3A showing spherical morphology under SEM, Figure 3B confirming the presence of C, O, and Ag through EDS, and Figure 3C presenting the corresponding elemental composition. For *C.C.*-AgNPs, Figure 4A showed similar SEM morphology, Figure 4B highlighted C, O, and Ag peaks in the EDS spectrum, and Figure 4C presented the percentage composition of the detected elements.

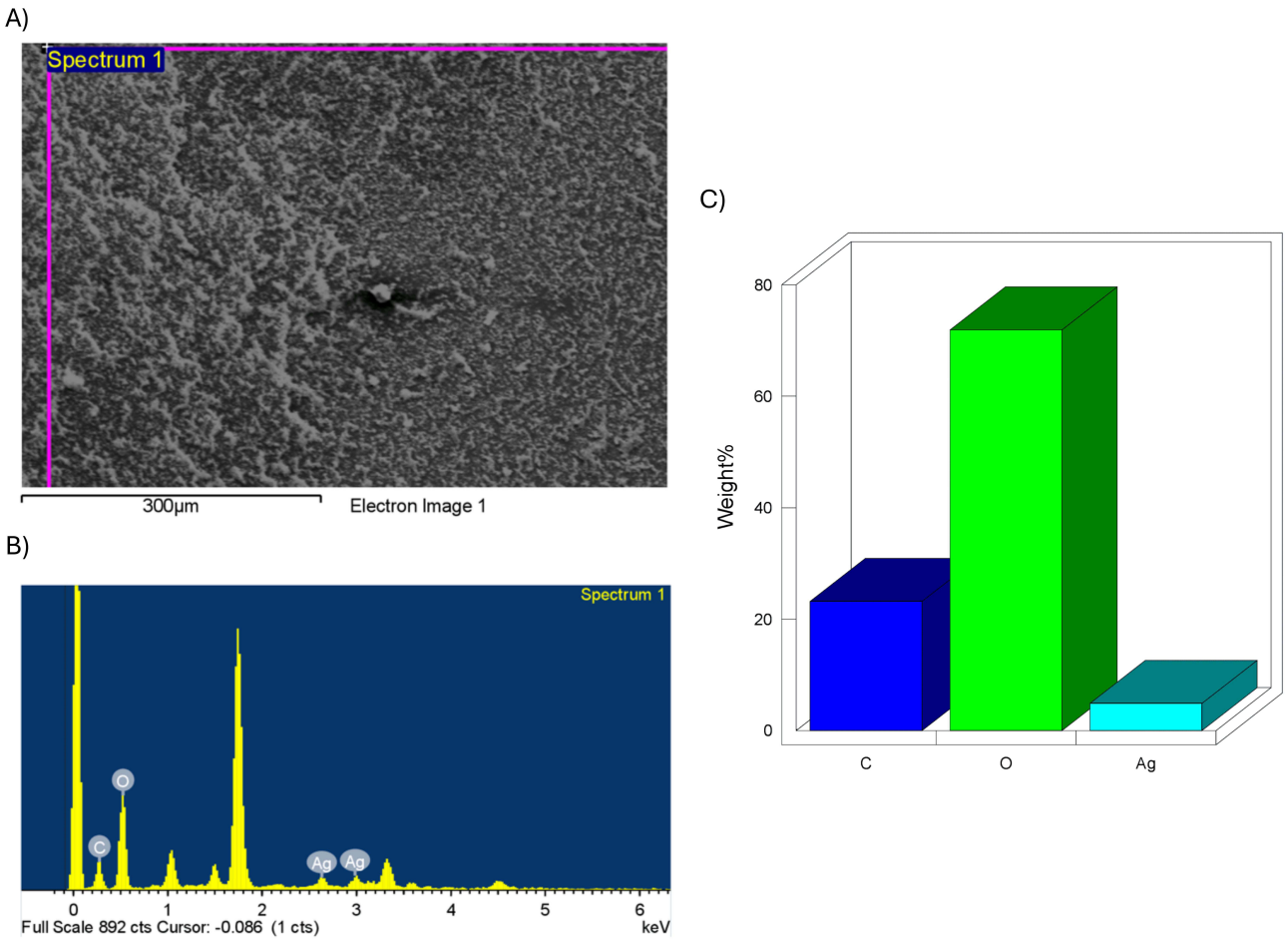

Figure 2 (**A**) SEM image (**B**) EDS spectrum (**C**) Percentage relative composition of elements in *R.S.*-AgNPs. (N=3).

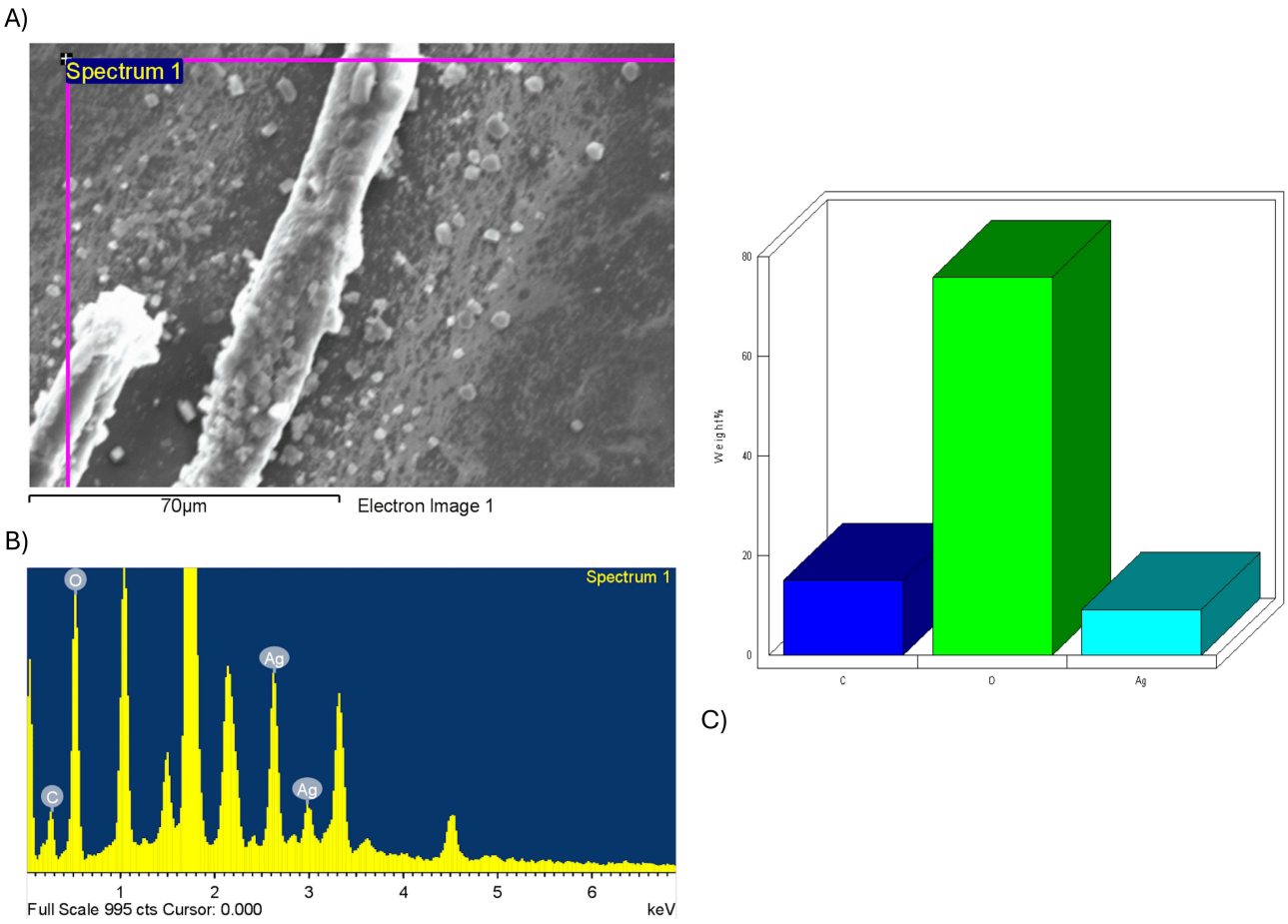

Figure 3 (**A**) SEM image (**B**) EDS spectrum (**C**) Percentage relative composition of elements in *C.P.*-AgNPs. (N=3).

FTIR Analysis

FTIR analysis was performed to identify the specific chemical compounds present in the interaction between silver nitrate and the plant extracts. For *R.S.*-AgNPs (Figure 5), the *R.S.* extract displayed absorption peaks at 3448.48 cm^{-1} and 1348.90 cm^{-1} (Figure 5A), while *R.S.*-AgNPs exhibited similar peaks with slight shifts at 3436.10 cm^{-1} and 1348.89 cm^{-1} (Figure 5B). The prominent peaks were attributed to polyphenols (hydroxyl groups) and amines (N-H stretching) near 3422 cm^{-1}, and nitro compounds (N-O symmetry stretching) near 1377 cm^{-1}. Similar patterns were observed for *C.P.*-AgNPs (Figure 6) and *C.C.*-AgNPs (Figure 7), with slight shifts in peak positions indicating the presence of phytochemicals that likely participated in the reduction and capping processes of the nanoparticles.

AgNPs Biological Activities

Anticancer

The cytotoxic effects of *R.S., C.P.*, and *C.C.*-AgNPs on MDA-MB231, KAIMRC-2, MCF-7, and MCF-10A cell lines were evaluated using an MTT assay and compared to the standard reference drug, Mitoxantrone. A dose-dependent cytotoxic response was observed in multiple cancer cell lines as shown in Figure 8. *R.S.*-AgNPs exhibited the highest cytotoxicity against MDA-MB231 cells (IC_{50} = 154.7 ± 7.76 µg/mL). *C.P.*-AgNPs exhibited the most potent cytotoxic activity against MCF-7 cells (IC_{50} = 121.2 ± 5.82 µg/mL), while *C.C.*-AgNPs showed the highest cytotoxicity against KAIMRC-2 cells (IC_{50} = 135.1 ± 3.87 µg/mL). Although Mitoxantrone exhibited higher cytotoxicity compared to the AgNPs, the *R.S., C.P.*, and *C.C.*-AgNPs demonstrated better safety profiles against the non-malignant MCF-10A cell line (IC_{50} values of 460.2 ± 13.89 µg/mL, 303.7 ± 10.24 µg/mL, and 429.1 ± 12.20 µg/mL, respectively) compared to Mitoxantrone (IC_{50} = 2.062 ± 10.05 µg/mL) as summarized in Table 1.

https://doi.org/10.2147/IJN.S516723

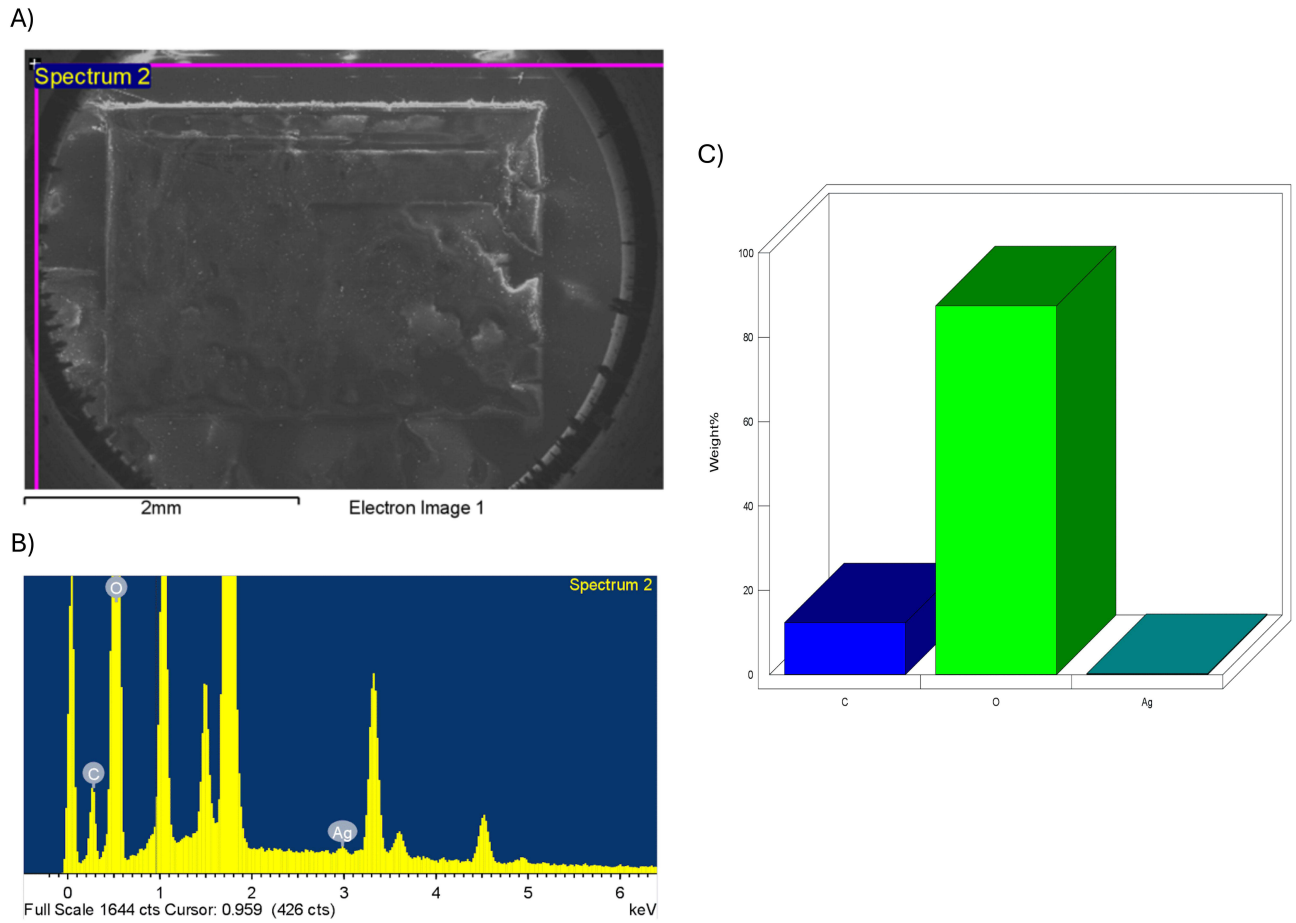

Figure 4 (**A**) SEM image (**B**) EDS spectrum (**C**) Percentage relative composition of elements in *C.C.*-AgNPs. (N=3).

Antibacterial

All types of AgNPs demonstrated effectiveness against the tested bacteria, *S. aureus* and *E. coli*. The inhibition zones were measured to determine their effectiveness (Figure 9). *R.S.*-AgNPs showed inhibition zones of 19 ± 0.82 mm (*S. aureus*) and 20.25 ± 0.50 mm (*E. coli), C.P.*-AgNPs displayed 18.50 ± 0.58 mm (*S. aureus*) and 17.25 ± 0.50 mm (*E. coli*), while *C.C.*-AgNPs exhibited 20.50 ± 0.58 mm (*S. aureus*) and 17.50 ± 0.58 mm (*E. coli*). Notably, the fabricated AgNPs were more effective than Ampicillin against both bacterial strains, with AgNPs showing larger inhibition zones compared to Ampicillin for both *S. aureus* and *E. coli* (****$p < 0.0001$), as illustrated in Table 1. Notably, an alpha level of 0.05 was established as the threshold for statistical significance in the analysis.

Identification of Bioactive R.S., C.P., and C.C. Metabolites

LC-MS analysis was performed to identify the major compounds in the plant extracts (Table 2) (Figure 10–12). The identification was based on predicted mass-to-charge ratios, accurate mass values, and confirmed by previously reported literature data. *R.S.* extract revealed multiple metabolites belonging to the alkaloid chemical class. Most metabolites in the *C.P.* extract belonged to the cardenolide class, with exceptions being Kaempferol-3-rutinoside, Rutin, and Isorhamnetin-Hexoside (flavonol glycosides). All identified metabolites in the *C.C.* extracts were considered to be polyphenolic compounds. These findings provide insight into the potential bioactive compounds responsible for the observed anticancer and antibacterial activities of the synthesized AgNPs.

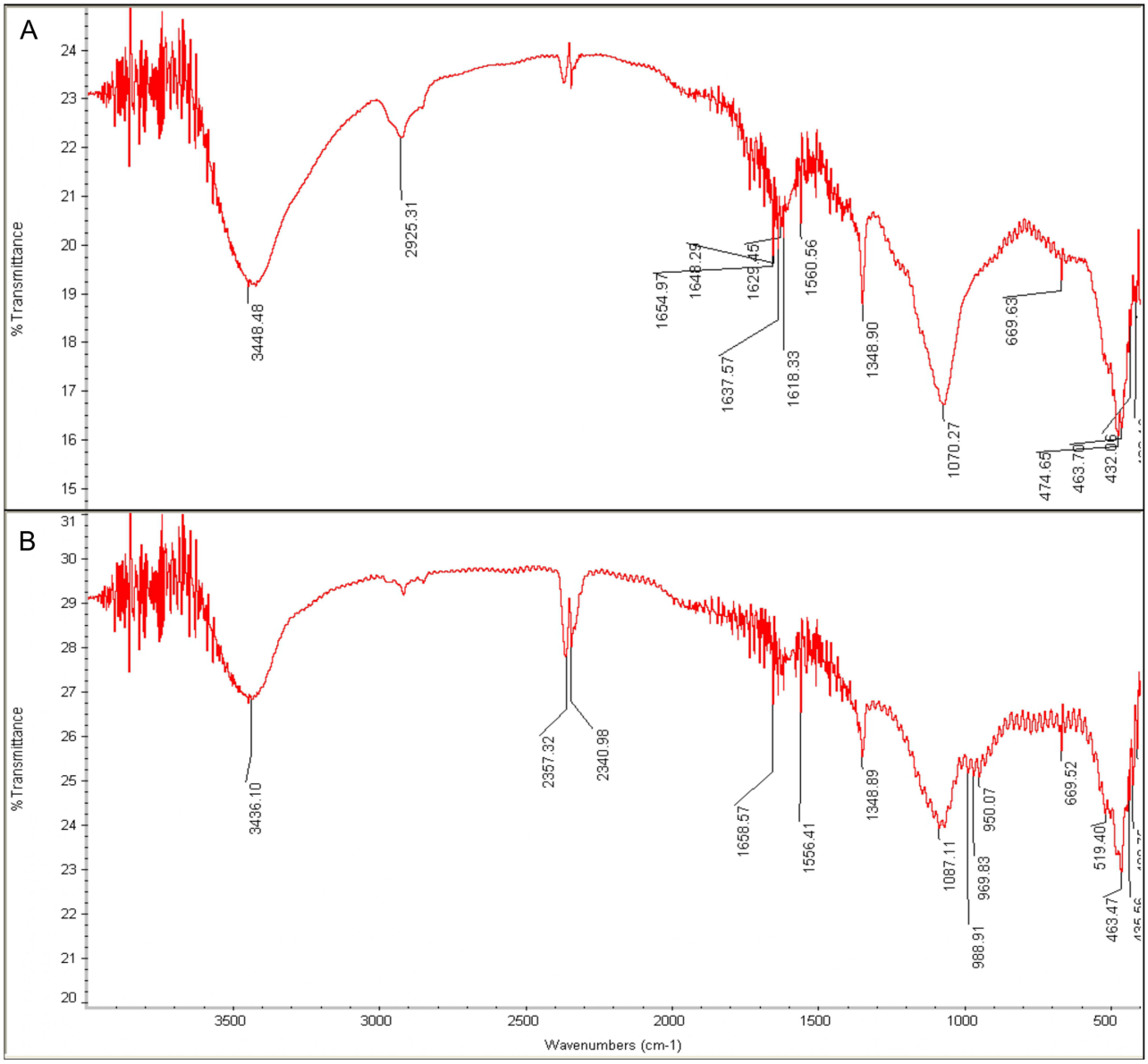

Figure 5 (**A**) FTIR analysis of *R.S.* extract and (**B**) *R.S.*-AgNPs obtained using an aqueous extract of *R.S.* (N=3).

In Silico Predictions of Secondary Metabolites Pharmacological Properties

Prediction of Anticancer Activity Using PASS Online Web Server

The investigation of plant metabolites for their potential as novel anticancer agents has gained significant attention in recent years. Previous studies have demonstrated promising anticancer activity in *R.S., C.P.*, and *C.C.* metabolites.[3,16–19] Assessing the anticancer activity of these metabolites is crucial for identifying promising candidates for further development, potentially leading to improved therapies with fewer side effects and economic benefits for the pharmaceutical industry. To evaluate the potential anticancer activities of *R.S., C.P.*, and *C.C.* metabolites, we employed the PASS. Our analysis revealed that 15-β-OH-calactin exhibited the highest probability of anticancer activity, followed by 16-β-OH-calactin and other secondary metabolites present in the three extracts (Table 3). Notably, the position of the hydroxyl group in calactin was found to significantly impact its anticancer properties. This observation provides valuable insights into the structure-activity relationship (SAR) of calactin, which can guide further research and development of potential anticancer agents.

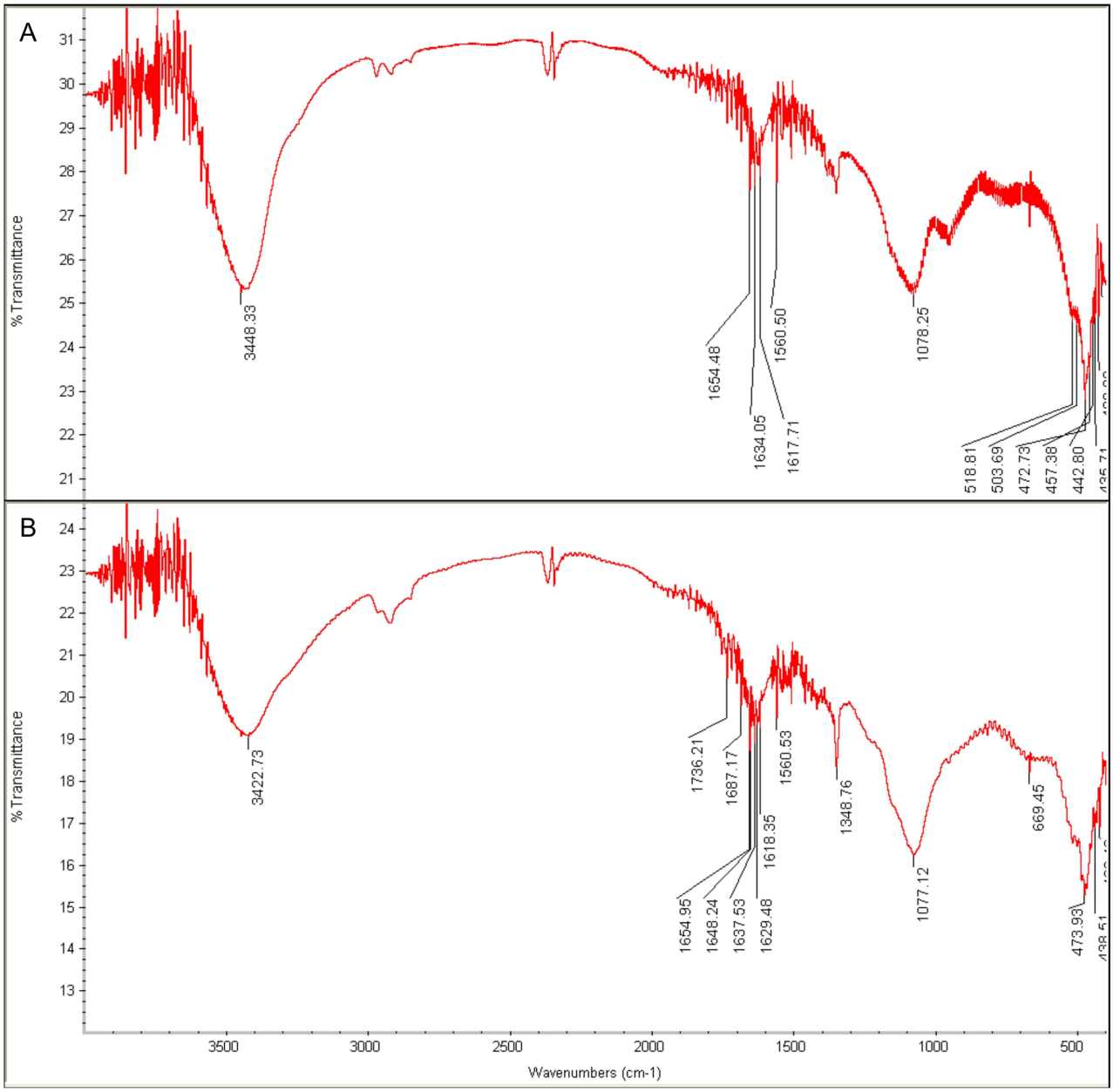

Figure 6 (**A**) FTIR analysis of *C.P.* extract and (**B**) *C.P.*-AgNPs obtained using an aqueous extract of *C.P.* (N=3).

Predictions of ADME Properties

The assessment of ADME properties is crucial in drug discovery and development. Promising cancer treatments should possess specific ADME characteristics, including small molecular weight, lipophilicity to penetrate the blood-brain barrier, high solubility, and P-glycoprotein substrate function. These properties can enhance a drug's pharmacokinetics and pharmacodynamics, improving efficacy, safety, and targeted delivery. Molecules with favorable ADME properties have a higher likelihood of success in clinical trials. We utilized SwissADME to predict the ADME properties of 19 metabolites from *R.S., C.P.*, and *C.C.* (Table 4). Our analysis revealed that all metabolites except Uzarigenin, Isorhamnetin-O-Hexoside, Apigenin-7-o-glucoside, Cirsiliol, Chlorogenic acid, Acacetin, Acetylaspidospermidine, and 15beta-Hydroxyvincadifformine exceeded 500 Da. 1-Acetylaspidospermidine demonstrated the highest lipophilicity while maintaining acceptable solubility, enabling effective blood-brain barrier permeation and high gastrointestinal (G. I). absorption. Eight metabolites showed poor/moderate water solubility, high G.I. absorption, and blood-brain barrier

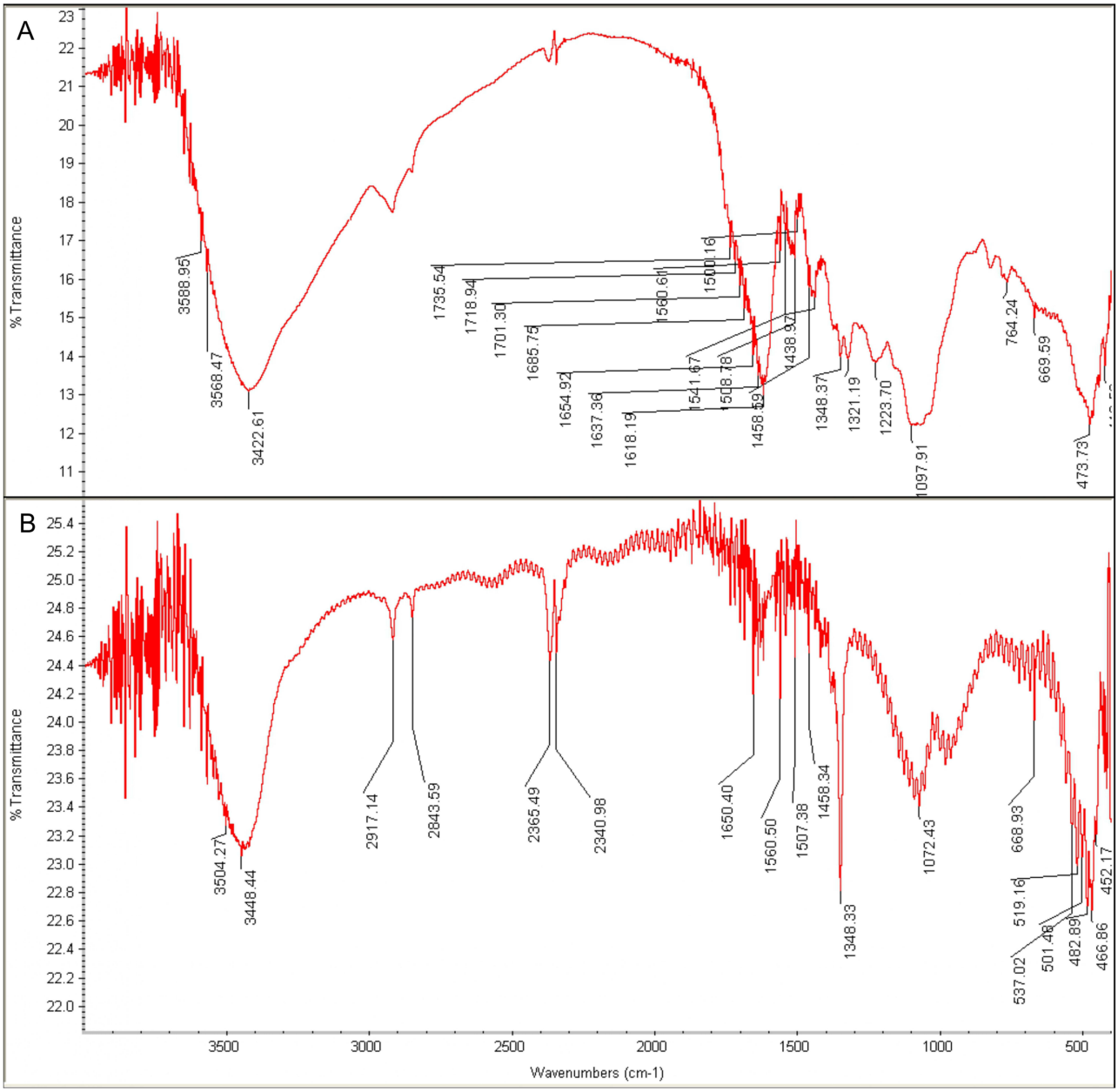

Figure 7 (**A**) FTIR analysis of *C.C.* extract and (**B**) *C.C.*-AgNPs obtained using an aqueous extract of *C.C.* (N=3).

penetration, qualifying as P-gp substrates. Only four metabolites violated Lipinski's Rule of Five (RO5) and were excluded from further analysis. The remaining 15 metabolites followed the RO5, suggesting lower attrition rates during clinical trials and increased market potential.

CYP450 Enzymes Inhibition Profile

The concomitant use of natural herbs and prescribed medications may result in undesirable side effects or therapeutic failure due to herb-drug interactions. One proposed mechanism for these interactions is the inhibition or induction of CYP450 enzymes. We employed the SwissADME webserver to evaluate potential interactions between bioactive metabolites and CYP450 enzymes. Our analysis, presented in (Table 5), revealed that Cirsiliol and Acacetin exhibited inhibition of almost all CYP groups except CYP2C19. All *R.S.* metabolites showed inhibition of CYP2D6, potentially

https://doi.org/10.2147/IJN.S516723

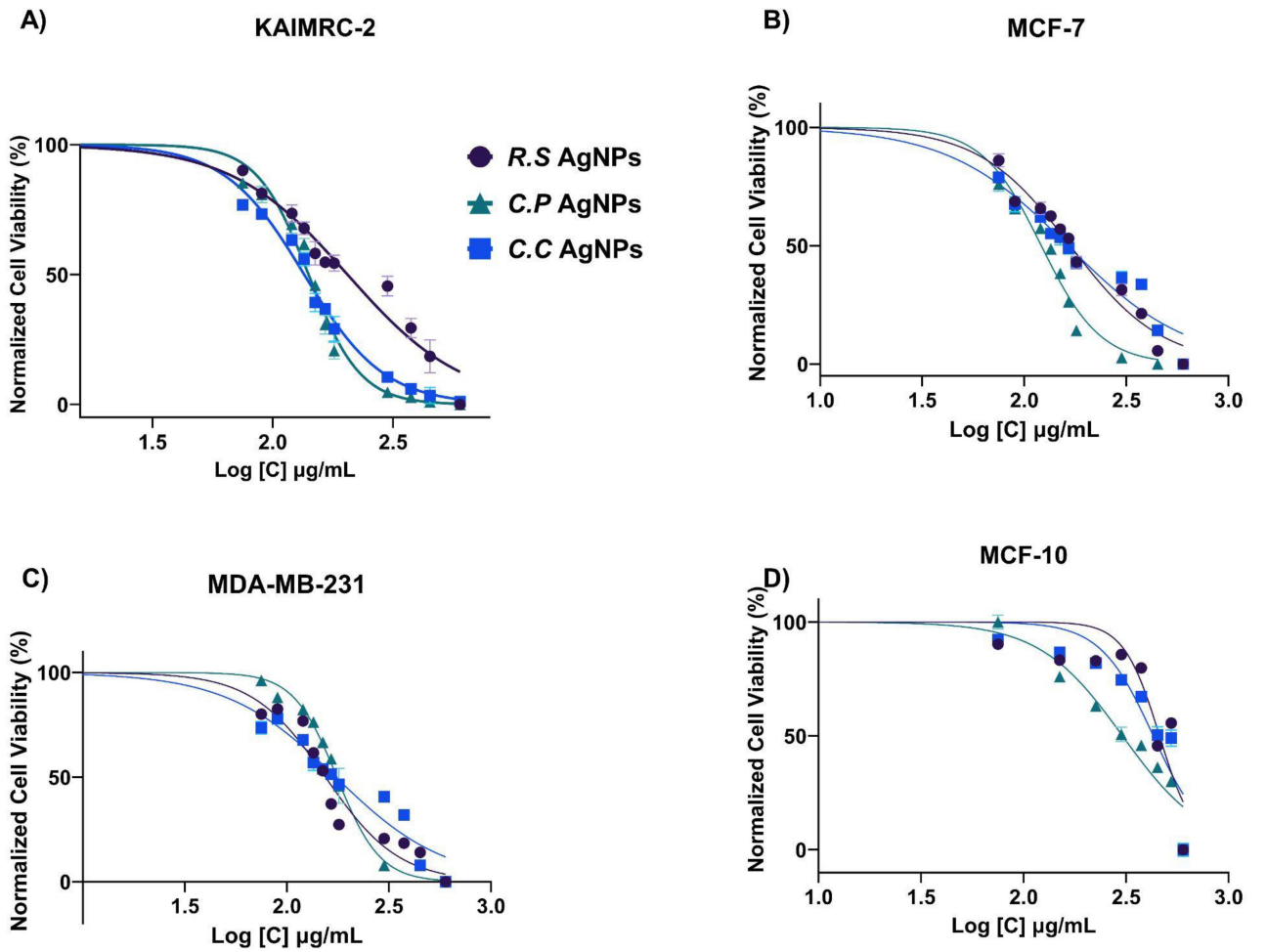

Figure 8 Dose-response showing the cytotoxic effect of *R.S.*, *C.P.*, and *C.C.*-AgNPs on the cell lines; (**A**) MDA-MB-231, (**B**) KAIMRC-2, (**C**) MCF-7, and (**D**) MCF-10A. (N=3).

affecting drugs metabolized by these enzymes. As a precautionary measure, metabolites inhibiting more than two CYP450 enzymes were excluded from further analysis to avoid potential herb-drug interactions.

Prediction of Organ and Endpoint Toxicity Analysis Using ProTox II

To predict oral toxicity levels for each metabolite, we utilized the ProTox-II web server. This tool provides rapid estimation of lethal dose (LD_{50}), organ toxicity (hepatotoxicity), and toxicity endpoints (carcinogenicity, immunotoxicity, mutagenicity, and cytotoxicity).[9] Toxicity prediction was run and computed for the 13 studied metabolites. As shown in Table 6, Our toxicity prediction analysis classified five metabolites as class 4 or 5, indicating they are either harmless or only mildly toxic if ingested. However, eight metabolites were classified as class 1 or 2, implying potential fatality or harm if swallowed. These were excluded from further analysis due to their toxic profile. Interestingly, the five remaining metabolites showed no hepatotoxicity or carcinogenicity and were found to be safe for human administration. This suggests that these metabolites have a promising pharmaceutical profile with potential for further exploration.

Prediction of Cardiotoxicity Using Pred-hERG 4.2 Online Web Server

We evaluated the cardiac toxicity potential of the secondary bioactive metabolites using the Pred-hERG web server, focusing on their impact on hERG potassium channels, known to cause cardiac issues like arrhythmia and mortality. Our analysis predicted that Voruscharin and Uscharin have potential cardiac toxicity, with confidence levels of 60% and 50% respectively. However, Apigenin-7-o-glucoside, 1-Acetylaspidospermidine, and Chlorogenic acid were predicted as non-

Table 1 (A) The IC_{50} of *R.S.*, *C.P.*, *C.C.*-AgNPs, and (B) the Mean Inhibition Zone of *R.S.*, *C.P.*, *C.C.*-AgNPs

(A) Anticancer Activity								
Name	**KAIMRC2 IC_{50} (μg/mL)**	**KAIMRC2 Standard Deviation of the Residuals (Sy.x)**	**MDA-MB231 IC_{50} (μg/mL)**	**MDA-MB231 Standard Deviation of the Residuals (Sy.x)**	**MCF-7 IC_{50} (μg/mL)**	**MCF-7 Standard Deviation of the Residuals (Sy.x)**	**MCF-10A IC_{50} (μg/mL)**	**MCF-10A Standard Deviation of the Residuals (Sy.x)**
R.S.-AgNPs	204.4	± 6.51	154.7	± 7.76	168.1	± 5.62	460.2	± 13.89
C.P.-AgNPs	140.8	± 4.71	175.9	± 4.98	121.2	± 5.82	303.7	± 10.24
C.C.-AgNPs	135.1	± 3.87	173.7	± 7.44	163.5	± 6.53	429.1	± 12.20
Mitoxantrone	1.30	± 12.62	1.67	± 11.92	1.27	± 9.11	2.06	± 10.05

(B) Antibacterial Activity				
Name	***S. aureus***		***E. coli***	
	Mean Inhibition Zone (mm)	**Standard Deviation (Sy.x)**	**Mean Inhibition Zone (mm)**	**Standard Deviation (Sy.x)**
R.S.-AgNPs	19.00	± 0.82	20.25	± 0.50
C.P.-AgNPs	18.50	± 0.58	17.25	± 0.50
C.C.-AgNPs	20.50	± 0.58	17.50	± 0.58
Ampicillin	13.25	± 0.50	12.50	± 0.58

https://doi.org/10.2147/IJN.S516723

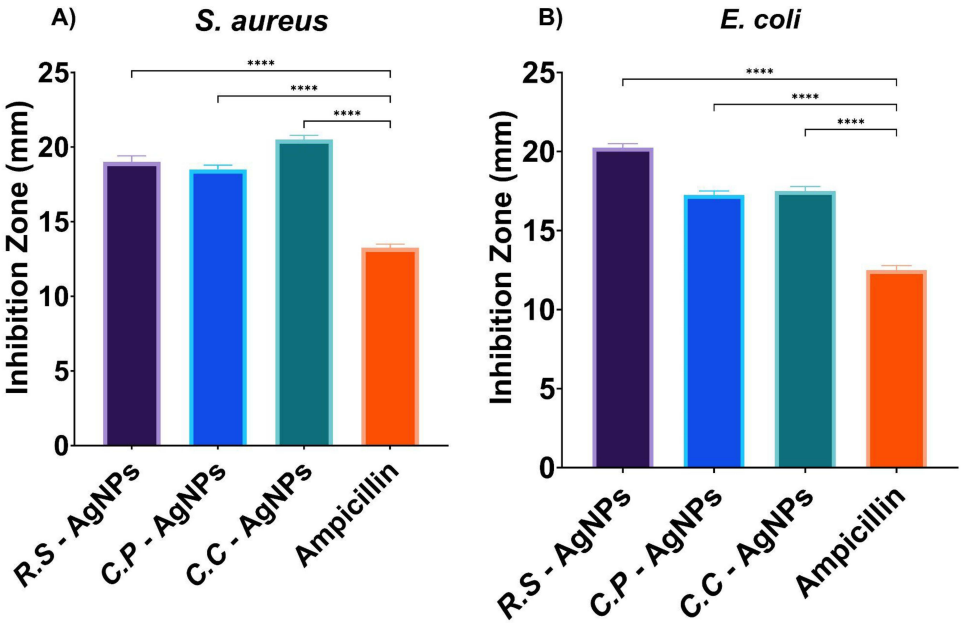

Figure 9 Antimicrobial activity of the synthesized *R.S., C.P., C.C.*-AgNPs, and Ampicillin against (**A**) *S. aureus* and (**B**) *E. coli* (N=3) *P*-value are represented as **** $p < 0.0001$.

cardiotoxic with confidence levels of 50%. As a precautionary measure, Voruscharin and Uscharin were excluded from further study due to potential cardiac risks.

Target Predictions

We employed two distinct web servers for target prediction: SWISS Target Prediction and Molinspiration, as demonstrated in (Table 7). Molinspiration indicates that compounds with bioavailability scores exceeding 0.00 are prospective

Table 2 Chemical Constituents of *R.S.*, *C.P.*, and *C.C.*

No	Name	Molecular Formula	MW (g/mol)	Precursor Type
		R.S.		
1	Rhazine[28]	$C_{21}H_{26}N_2O_3$	354	$[M+H]^+$ = 355.1943, found at 355.2057.
2	Tetrahydroalstonine[28]	$C_{21}H_{24}N_2O_3$	352	$[M+H]^+$ =353.1787, found at 355.2045.
3	15-β-Hydroxyvincadifformine[29]	$C_{21}H_{26}N_2O_3$	354	$[M+H]^+$ = 355.1943, found at 355.2050.
4	Vincamine[28]	$C_{21}H_{26}N_2O_3$	354	$[M+H]^+$ = 355.2013, found at 355.2056.
5	Rhazimanine[30]	$C_{21}H_{26}N_2O_3$	354	$[M+H]^+$ = 355.2013, found at 355.2050.
6	Stemmadenine[31]	$C_{21}H_{26}N_2O_3$	354	$[M+H]^+$ = 355.2013, found at 355.2057.
7	Ajmalicine[32]	$C_{21}H_{24}N_2O_3$	352	$[M+H]^+$ = 353.1857, found at 353.1897.
8	Yohimbine[28]	$C_{21}H_{26}N_2O_3$	354	$[M+H]^+$ = 355.2013, found at 355.2056.
9	Polyneuridine[31]	$C_{21}H_{24}N_2O_3$	352	$[M+H]^+$ = 353.1857, found at 353.1901.
10	Strictamine[31]	$C_{20}H_{22}N_2O_2$	322	$[M+H]^+$ = 323.1751, found at 323.1791.
11	Akuammidine[33]	$C_{21}H_{24}N_2O_3$	352	$[M+H]^+$ = 353.1857, found at 353.1904.
12	Condylocarpine[34]	$C_{20}H_{22}N_2O_2$	322	$[M+H]^+$ = 323.1751, found at 323.1791.

(*Continued*)

Table 2 (Continued).

No	Name	Molecular Formula	MW (g/mol)	Precursor Type
		C.P.		
1	Calactin[35]	$C_{29}H_{40}O_9$	532	$[M+Na]^+$ = 555.2672, found at 555.3635.
2	Calotropin[35]	$C_{29}H_{40}O_9$	532	$[M+NH_4]^+$ = 550.2672, found at 550.3344.
3	12-ß-OH-calactin[35]	$C_{29}H_{40}O_{10}$	548	$[M+NH_4]^+$ = 566.2621, found at 566.4349.
4	15-ß-OH-calactin[35]	$C_{29}H_{40}O_{10}$	548	$[M+NH_4]^+$ = 566.2621, found at 566.4349.
5	16-ß-OH-calactin[35]	$C_{29}H_{40}O_{10}$	548	$[M+NH_4]^+$ = 566.2621, found at 566.4349.
6	2”-Oxovoruscharin[35]	$C_{31}H_{41}NO_9S$	603	$[M+NH_4]^+$ = 621.2544, found at 621.1875.
7	Voruscharin[35]	$C_{31}H_{43}NO_8S$	603	$[M+NH_4]^+$ = 621.2544, found at 621.1875.
8	Asclepin[35]	$C_{31}H_{42}O_{10}$	574	$[M-Cl]^-$ = 539.2778, found at 539.4412.
9	Uscharin[35]	$C_{31}H_{41}NO_8S$	587	$[M+Na]^+$ = 610.2553, found at 610.9148.
10	Kaempferol-3-rutinoside[35]	$C_{27}H_{30}O_{15}$	594	$[M+Na]^+$ = 617.1585, found at 617.2134.
11	Rutin[35]	$C_{27}H_{30}O_{16}$	610	$[M+Na]^+$ = 633.1534, found at 633.1515.
12	Isorhamnetin-Hexoside[35]	$C_{22}H_{22}O_{12}$	478	$[M+K]^+$ = 517.1111, found at 517.3826.
		C.C.		
1	Catechin[36]	$C_{15}H_{14}O_6$	290	$[M+Na]^+$ =313.0790, found at 313.0199.
2	Apigenin 7-*O*-glucoside[36]	$C_{21}H_{20}O_{10}$	432	$[M+H]^+$ = 433.1056, found at 433.1198.
3	Cirsiliol[36]	$C_{17}H_{14}O_7$	330	$[M+Na]^+$ =353.1925, found at 353.1918.
4	Epicatechin flavanol[36]	$C_{15}H_{14}O_6$	290	[M+Na]+ =313.0790, found at 313.0199.
5	Acacetin[36]	$C_{16}H_{12}O_5$	284	$[M+Na]^+$ = 307.0013, found at 307.0013.
6	4,5,Dicaffeoylquinic acid[37]	$C_{25}H_{24}O_{12}$	516	$[M+H]^+$ = 517.1268, found at 517.3821.
7	Chlorogenic acid[36]	$C_{16}H_{18}O_9$	354	$[M+NH_4]^+$ = 372.0951, found at 372.2240.

bioactive compounds. The SWISS Target Prediction analysis identified Apigenin-7-o-glucoside as a potential treatment for breast cancer by targeting TNF-α, a cytokine that plays a significant role in promoting tumor growth, angiogenesis, and metastasis.[29] 1-Acetylaspidospermidine was found to target Family A G protein-coupled receptor, which is involved in various cellular processes crucial in cancer development and progression.[30] Additionally, Chlorogenic acid was found to target aldose reductase, an enzyme implicated in the development of diabetic complications and cancer progression, including breast cancer.[31] The Molinspiration analysis suggests that Apigenin-7-o-glucoside may have multiple targets, including GPCR ligands, kinase inhibitors, nuclear inhibitors, protease inhibitors, and enzyme inhibitors. These targets are intricately associated with various cellular processes and signaling pathways that play a crucial role in cancer progression. However, 1-Acetylaspidospermidine and Chlorogenic acid target ion channel modulators but not kinase inhibitors. These findings provide valuable insights into the potential anticancer properties and mechanisms of action of the studied metabolites, paving the way for further investigation and development of novel cancer therapeutics.

Discussion

AgNP Properties

NPs possess unique physical, chemical, and biological properties that distinguish them from their bulk origins. These characteristics include specialized crystal structures, targeted delivery capabilities, and controlled release mechanisms, which have facilitated the rapid growth of NP applications in fields such as drug delivery, aesthetics, tissue engineering, theranostics, and agriculture.[32] AgNPs have garnered particular attention due to their diverse applications, including antimicrobial, antioxidant, and anticancer activities, as well as their role in enhancing vaccine immunogenicity.[33]

In our study, the successful synthesis of AgNPs validated through TEM and DLS imaging, which revealed a range of particle sizes across the three plant extracts. *R.S.*- AgNPs produced the largest nanoparticles, followed by *C.P.*-AgNPs,

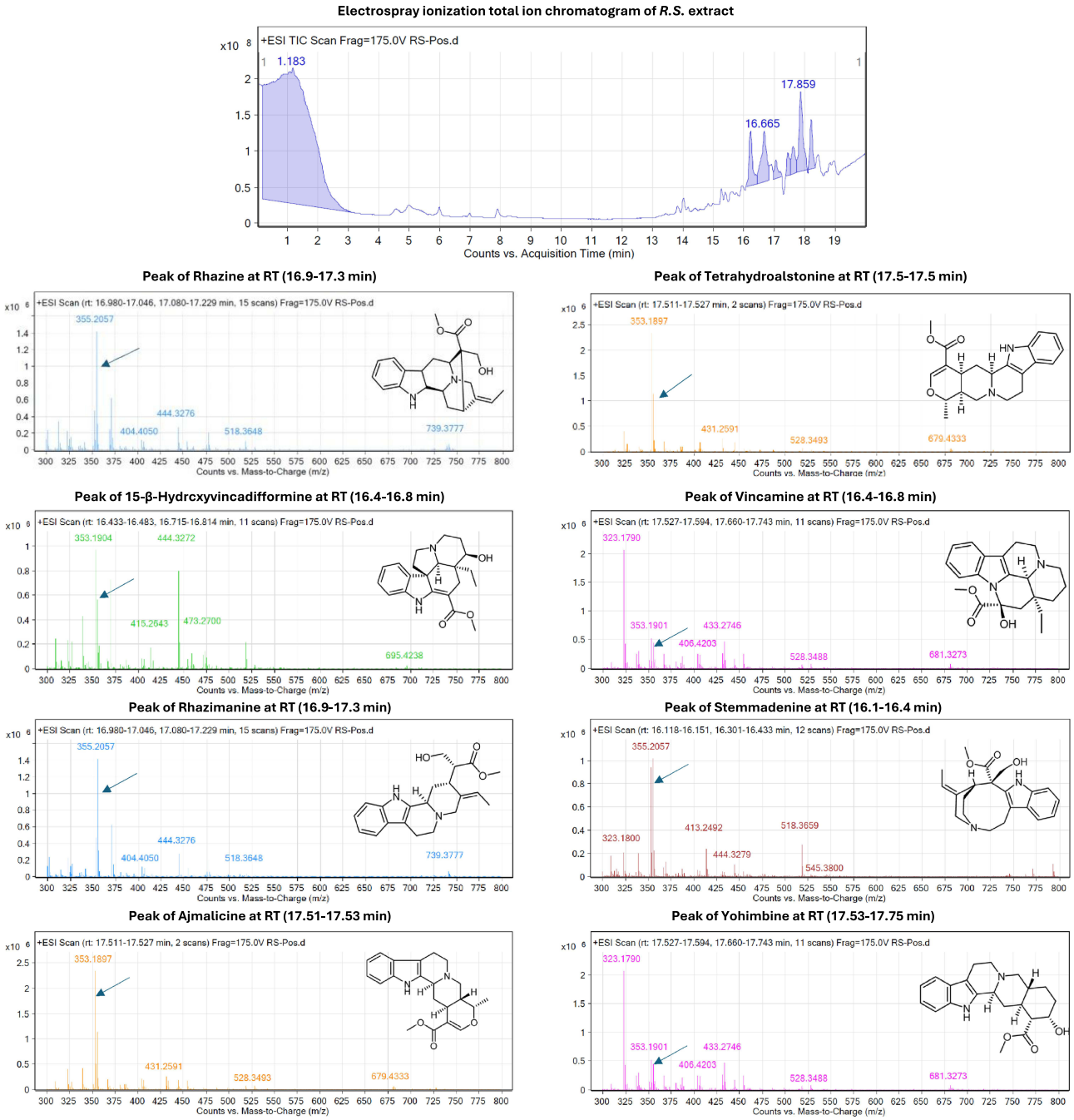

Figure 10 Conitnued.

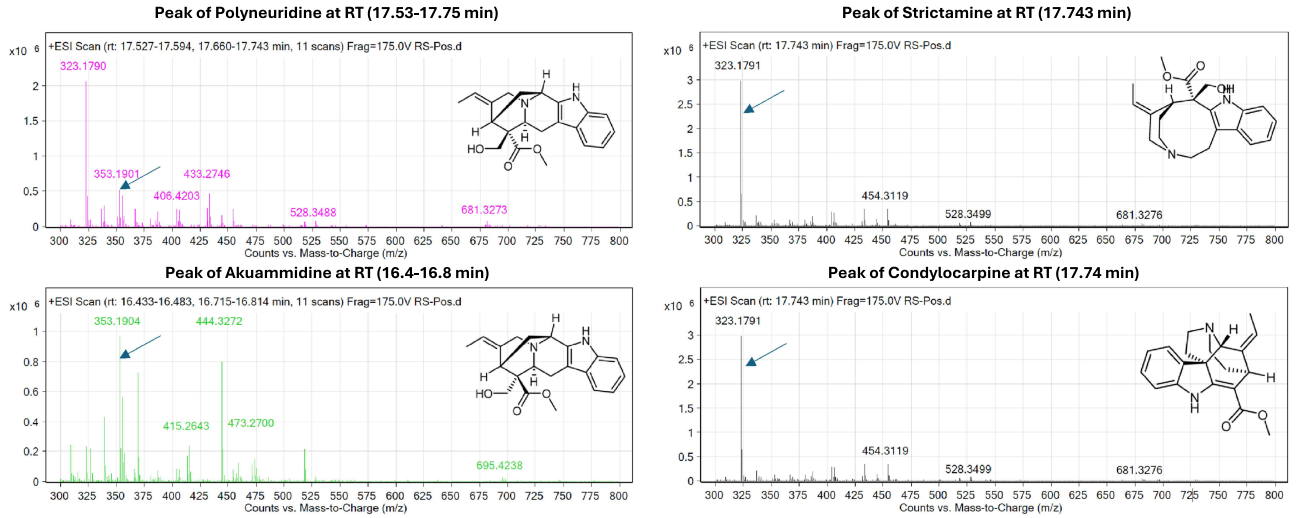

Figure 10 Base peak chromatogram of *R.S.* aqueous extract and their tentatively recognized biomolecules (indicated by blue arrows).

and *C.C.*-AgNPs generating the smallest. These size variations could be attributed to differences in phytochemical composition and reducing agent type and concentration in each extract, influencing the nanoparticle formation process.[34]

EDS was employed to study the elemental compositions of *R.S., C.P.*, and *C.C.*-AgNPs, while SEM microphotographs evaluated their morphology, revealing non-aggregated and predominantly spherical shapes, indicating successful reduction. EDS analysis displayed distinct peaks for carbon and oxygen, suggesting efficient capping of AgNPs by carbon-based phytochemicals and plant metabolites that serve as stabilizing agents in NP formation.[35]

FTIR analysis revealed similar chemical compounds in both synthesized AgNPs and their respective plant extracts (*R.S., C.P.*, and *C.C)*. The similarity in absorption peaks between the extracts and the corresponding AgNPs strongly suggests that phytochemicals present in the plant extracts played a significant role in the AgNP reduction and capping processes.

Common peaks, observed around 3422 cm^{-1}, were attributed to polyphenols (hydroxyl groups) and amines (N-H stretching). Peaks near 1377 cm^{-1} indicated the presence of nitro compounds (N-O symmetric stretching). Specifically, *R.S.*-AgNPs and the *R.S.* extract displayed peaks consistent with polyphenols, amines, and nitro compounds, aligning with previous findings by Rahman et al,[36] who identified hydroxyl, carboxyl, carbonyl, and amide groups in *R.S.*-AgNPs. Al-Sahli et al[37] reported the presence of hydroxyl, nitrile, amine, conjugated ketone, and sulfate functional groups in R.S.-AgNPs extract.

Furthermore, *C.P.*-AgNPs and *C.P.* extract exhibited peaks associated with polyphenols and sulfoxide compounds. *C.C.*-AgNPs and *C.C.* extract showed peaks corresponding to polyphenols, amines, and nitro compounds. An additional study identified OH stretching, C–H groups, N-H stretching, C–H bending, C–N stretching, C–O stretching (indicative of carboxylic acid groups), and C-H alkyne bands in *C.P.*-AgNPs.[38] These consistent findings across multiple analyses strongly support the role of plant-derived phytochemicals in the AgNP synthesis. Although the plant extract served as a green and cost-effective reducing and stabilizing agent, variation in its phytochemical composition could impact the reproducibility of AgNPs synthesis and biological activity. Further research should focus on standardizing the synthesis process to ensure batch-to-batch consistency.

AgNP Biological Activity

Anticancer Activity

Our study found that *C.P.*-AgNPs exhibited greater cytotoxicity against MCF-7 cells with an IC_{50} of 121.2 µg/mL, compared to the findings of Alghamdi et al,[21] who found that various concentration of ethyl acetate extract of *C.P.* (125 µg/mL and 250 µg/mL) inhibiting the growth of both KAIMRC2 and HCT8 (the colorectal cancer cell line) cell lines.

https://doi.org/10.2147/IJN.S516723

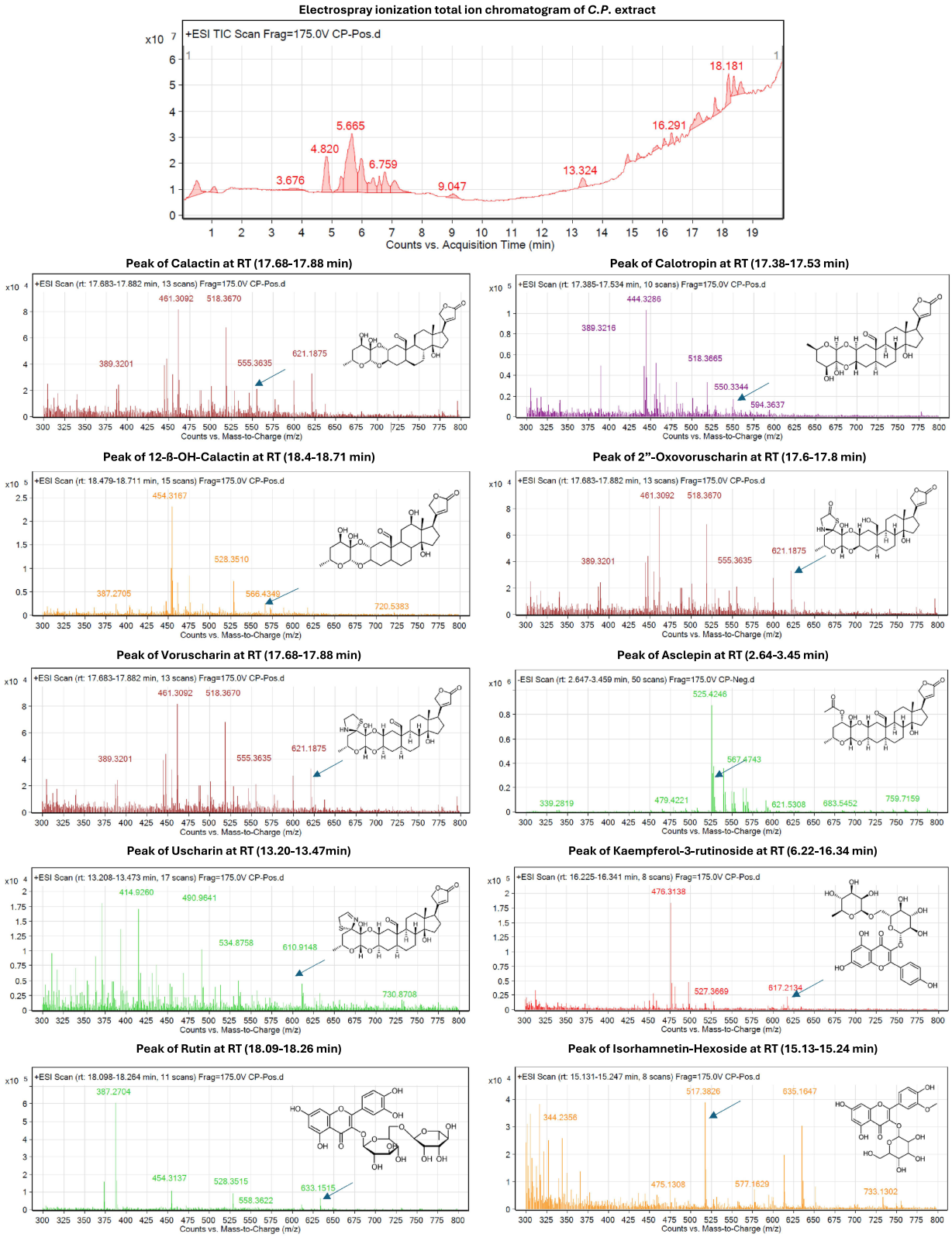

Figure 11 Base peak chromatogram of *C.P.* aqueous extract and their tentatively recognized biomolecules (indicated by blue arrows).

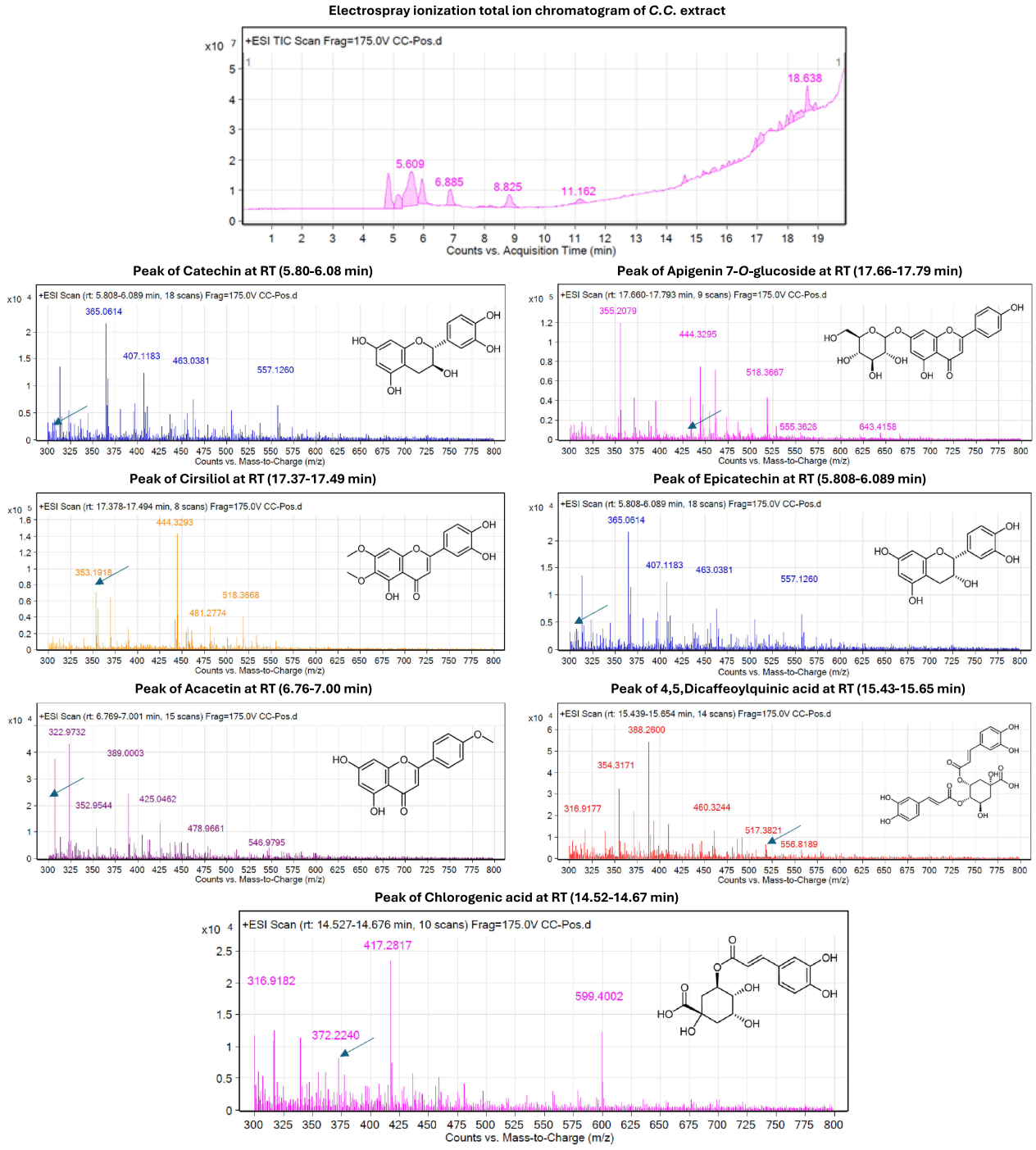

Figure 12 Base peak chromatogram of *C.C.* aqueous extract and their tentatively recognized biomolecules (indicated by blue arrows).

However, at these concentrations, KAIMRC2 cells demonstrated a greater propensity for apoptosis compared to HCT8 cells.

Additionally, we observed that *C.C.*-AgNPs showed an IC_{50} of 135.1 µg/mL against KAIMRC-2 cells, whereas Alghamdi et al[39] reported an IC_{50} of 54.97 µg/mL for the ethanolic *C.C.* extract against the same cell line. These variations in IC_{50} values may be attributed to the distinct solvent system (which would affect the presence of metabolites) used in preparation of reported extract and our silver nanoparticles. Our experiments assessed acute cytotoxic effects over a short period, which may not fully capture long-term drug resistance or adaptive responses that could occur in a clinical

https://doi.org/10.2147/IJN.S516723

Table 3 Secondary Metabolites with High Likelihood to Exhibited Anticancer Activity Using PASS Online Webserver

N	Plant Name	Metabolite Name	Pa
1	*R.S.*	15beta-Hydroxyvincadifformine	0.792
2		Acetylaspidospermidine	0.769
3	*C.P.*	15-ß-OH-calactin	0.962
4		16-ß-OH-calactin	0.957
5		Voruscharin	0.957
6		Uscharin	0.955
7		Calactin	0.950
8		Calotropin	0.95
9		12-ß-OH-calactin	0.946
10		Asclepin	0.946
11		Kaempferol-3-Rutinoside	0.851
12		Rutin	0.849
13		Uzarigenin	0.835
14		Isorhamnetin-O-Hexoside	0.834
15	*C.C.*	Apigenin-7-O-glucoside	0.828
16		Cirsiliol	0.819
17		4,5-Dicaffeoylquinicacid	0.790
18		Chlorogenic acid	0.776
19		Acacetin	0.755

Table 4 The Prediction Results of ADME Parameters, Pharmacokinetic Properties, and Drug-Likeness of the Metabolites with High Likelihood to Exhibited Anticancer Activity

Plant Name	Metabolites Name	MW (g/mol)	HB Donor	HB Acceptor	Lipophilicity Log $P_{o/w}$ (XLOGP)	Water Solubility Log S (SILICOS-IT)	G.I. Absorption	B.B.B. Permeant	P-gp Substrate	Drug-Likeness Lipinski Rule
R.S.	1-Acetylaspidospermidine	324.46	2	2	3.40	−4.73	High	Yes	Yes	Yes; 0 violation
	15 beta-Hydroxyvincadifformine	354.44	2	4	2.51	−4.56	High	Yes	Yes	Yes; 0 violation
C.P.	Calactin	532.62	3	9	0.93	−2.35	High	No	Yes	Yes; 1 violation
	Calotropin	532.62	3	9	0.93	−2.35	High	No	Yes	Yes; 1 violation
	Uzarigenin	374.51	2	4	2.64	−3.46	High	Yes	Yes	Yes; 0 violation
	12-ß-OH-calactin	548.62	4	10	−0.23	−1.52	Low	No	Yes	Yes; 1 violation
	16-ß-OH-calactin	548.62	4	10	−0.05	−1.52	Low	No	Yes	Yes; 1 violation

(*Continued*)

Table 4 (Continued).

Plant Name	Metabolites Name	MW (g/mol)	HB Donor	HB Acceptor	Lipophilicity Log $P_{o/w}$ (XLOGP)	Water Solubility Log S (SILICOS-IT)	G.I. Absorption	B.B.B. Permeant	P-gp Substrate	Drug-Likeness Lipinski Rule
C.P.	15-ß-OH-calactin	548.62	4	10	−0.05	−1.52	Low	No	Yes	Yes; 1 violation
	Voruscharin	589.74	3	9	1.52	−3.78	Low	No	Yes	Yes; 1 violation
	Asclepin	574.66	2	10	1.50	−2.95	High	No	Yes	Yes; 1 violation
	Uscharin	587.72	2	9	1.36	−3.55	Low	No	Yes	Yes; 1 violation
	Kaempferol-3-rutinoside	594.52	9	15	0.02	−0.88	Low	No	Yes	No; 3 violation
	Rutin	610.52	10	16	−0.33	−0.29	Low	No	Yes	No; 3 violation
	Isorhamnetin-O-Hexoside	478.40	7	12	0.69	−2.20	Low	No	No	No; 2 violation
C.C.	Apigenin-7-o-glucoside	432.38	6	10	1.81	−2.69	Low	No	Yes	Yes; 1 violation
	Cirsiliol	330.3	3	7	3.07	−4.63	High	No	No	Yes; 0 violation
	4,5-Dicaffeoylquinic acid	516.45	7	12	1.52	−1.16	Low	No	Yes	No; 3 violations
	Chlorogenic acid	354.31	6	9	−0.42	0.40	Low	No	No	Yes; 1 violation
	Acacetin	284.2	2	5	3.35	−5.10	High	No	No	Yes; 0 violation

Table 5 CYP-P450 Enzyme Inhibition of Metabolites According to SwissADME Webserver

Plant Name	Metabolite Name	CYP Inhibition (CYP1A2, CYP2C19, CYP2C9, CYP2D6, CYP3A4)
R.S.	15beta-Hydroxyvincad	CYP2D6 inhibitor
	Ifformine	CYP2D6 inhibitor
	Acetylaspidos	CYP2D6 inhibitor
	Permidine	CYP2D6 inhibitor
C.P.	15-ß-OH-calactin	No
	16-ß-OH-calactin	No
	Voruscharin	No
	Uscharin	No
	Calactin	No
	Calotropin	No
	12-ß-OH-calactin	No
	Asclepin	No
	Uzarigenin	No
C.C.	Apigenin-7-o-glucoside	No
	Cirsiliol	Inhibit all CYP except CYP2C19
	Chlorogenic acid	NO
	Acacetin	Inhibit all CYP except CYP2C19

https://doi.org/10.2147/IJN.S516723

Table 6 Organ and Endpoints Evaluated Toxicity for the Studied Metabolites Using the ProTox-II

Plant Name	Metabolites	LD_{50}	Toxicity Class	Hepatotoxicity (Probability)	Toxicity Endpoint & Probability			
					Carcinogenicity (Probability)	Immunotoxicity (Probability)	Mutagenicity (Probability)	Cytotoxicity (Probability)
R.S.	1- Acetylaspidospermidine	325mg/kg	Class 4	Inactive (0.89)	Inactive (0.69)	Inactive (0.89)	Inactive (0.72)	Inactive (0.73)
	15beta-Hydroxyvincadifformine	1mg/kg	Class 1	Inactive (0.83)	Active (0.51)	Inactive (0.61)	Inactive (0.67)	Inactive (0.54)
C.P.	Calactin	8mg/kg	Class 2	Inactive (0.94)	Inactive (0.69)	Active (0.99)	Inactive (0.80)	Active (0.99)
	Calotropin	8mg/kg	Class 2	Inactive (0.94)	Inactive (0.69)	Active (0.99)	Inactive (0.80)	Active (0.99)
	Uzarigenin	26mg/kg	Class 2	Inactive (0.73)	Inactive (0.67)	Active (0.99)	Inactive (0.79)	inactive (0.58)
	12-ß-OH-calactin	8mg/kg	Class 2	Inactive (0.95)	Inactive (0.74)	Active (0.99)	Inactive (0.77)	Active (0.97)
	16-ß-OH-calactin	41mg/kg	Class 2	Inactive (0.95)	Inactive (0.74)	Active (0.99)	Inactive (0.77)	Active (0.97)
	15-ß-OH-calactin	8mg/kg	Class 2	Inactive (0.94)	Inactive (0.69)	Active (0.99)	Inactive (0.80)	Active (0.99
	Voruscharin	3500mg/kg	Class 5	Inactive (0.82)	Inactive (0.59)	Active (0.99)	Inactive (0.64)	Active (0.57)
	Asclepin	9mg/kg	Class 2	Inactive (0.95)	Inactive (0.61)	Active (0.99)	Inactive (0.90)	Active (0.94)
	Uscharin	2000mg/kg	Class 4	Inactive (0.82)	Inactive (0.58)	Active (0.99)	Inactive (0.67)	Active (0.76)
C.C.	Apigenin-7-o-glucoside	5000mg/kg	Class 5	Inactive (0.82)	Inactive (0.86)	Inactive (0.93)	Active (0.59)	Inactive (0.69)
	Chlorogenic acid	5000mg/kg	Class 5	Inactive (0.72)	Inactive (0.68)	Active (0.99)	Inactive (0.93)	Inactive (0.80)

Notes: Color codes: dark red = toxic (high confidence), light red = toxic (low confidence); dark green = non-toxic (high confidence), light green = non-toxic (low confidence).

Table 7 The Predicted Biological Targets Involved in Mediating Studied Metabolites Anti-Cancer Activity Using SWISS Target Prediction, and Molinspiration Web Servers

Metabolite Name	Target Predictions		
	SWISS Target Prediction	Molinspiration	
1- Acetylaspidospermidine	Family A G protein-coupled receptor	GPCR ligand	0.32
		Ion channel modulator	0.03
		Kinase inhibitor	−0.39
		Nuclear receptor ligand	0.06
		Protease inhibitor	0.25
		Enzyme inhibitor	0.05

(*Continued*)

Table 7 (Continued).

Metabolite Name	Target Predictions		
	SWISS Target Prediction	Molinspiration	
Apigenin-7-o-glucoside	TNF-α	GPCR ligand	0.1
		Ion channel modulator	−0.01
		Kinase inhibitor	0.14
		Nuclear receptor ligand	0.31
		Protease inhibitor	0.02
		Enzyme inhibitor	0.43
Chlorogenic acid	Aldose reductase	GPCR ligand	0.29
		Ion channel modulator	0.14
		Kinase inhibitor	−0.00
		Nuclear receptor ligand	0.74
		Protease inhibitor	0.27
		Enzyme inhibitor	0.62

setting. Further research should include longer exposure times and repeated dosing studies to evaluate the potential for resistance development and sustained therapeutic effects.

Antibacterial Activity

Our findings demonstrated that *R.S.*-AgNPs exhibited antibacterial activity against *S. aureus* and *E. coli* with inhibition zones of 19 ± 0.82 mm and 20.25 ± 0.50 mm, respectively. These results are comparable to those reported by Rahman et al,[36] who found inhibition zones of 20 ± 0.73 mm and 22 ± 0.37 mm of *R.S.*-AgNPs against *S. aureus* and *E. coli*, respectively. Notably, *R.S.*-AgNPs showed superior antibacterial activity compared to the standard control, Ampicillin, which aligns with the findings of Rahman et al[36] when compared to cefixime. Moreover, Alghamdi et al[21] found that chloroform extraction of *R.S.* exhibited the highest activity against *S. aureus* with an inhibition zone of 14.3 ± 0.9 compared to water and ethyl acetate extracts.

C.P.-AgNPs demonstrated antibacterial activity against *E. coli* with an inhibition zone of 17.25 ± 0.50 mm, correlating with the findings of Sagadevan et al,[40] who found an inhibition zone of 17 ± 0.9 mm of *C.P.*-AgNPs at 100 µg concentration against *E. coli*. Additionally, in our previous work Alghamdi et al[21] found an inhibition zone of 13.5 ± 1.7 mm of ethyl acetate extraction of *C.P.* against *S. aureus*, whereas our results showed that *C.P.*-AgNPs showed an inhibition zone of 18.50 ± 0.5774 mm against *S. aureus.*

C.C.-AgNPs exhibited higher antibacterial activity against *E. coli* compared to Ampicillin, while Algebaly et al[41] reported higher activity compared to Amoxicillin. Both studies observed higher antibacterial activity against *S. aureus*, highlighting the consistent efficacy of *C.C.*-AgNPs against gram-positive bacteria while underscoring its variable performance against gram-negative organisms like *E. coli*. Our study only compared the nanoparticles to a single conventional antibiotic (Ampicillin). While this provides an initial benchmark, further studies should compare AgNPs against a broader range of antibiotics to better assess their relative potency.

Metabolites

LC-MS analysis of *R.S., C.P., and C.C.* extracts revealed multiple metabolites. *R.S.* extract metabolites predominantly belonged to the alkaloid class, demonstrating enhanced anticancer activity against human breast cancer, consistent with the findings of Nabih et al.[9] *C.P.* metabolites were primarily cardenolides, with the exception of Kaempferol-3-rutinoside,

Rutin, and Isorhamnetin-Hexoside, which are flavonol glycosides, correlating with the finding of Wadhwani et al,[42] who found flavonoid glycosides, steroids and cardenolides. *C.C*. extract metabolites were predominantly polyphenolic compounds.

In silico Evaluation of Secondary Metabolites Pharmacological Properties

Using the PASS online webserver, we found that 15-β-OH-calactin demonstrated the greatest potential for anticarcinogenic and antineoplastic activity, followed by 16-β-OH-calactin. These results align with the findings of Wadhwani et al,[42] who reported that 15-β-OH-hydroxy calactin exhibited the highest cytotoxic activity. The alteration in the position of the hydroxyl group was found to adversely affect the anticancer properties of calactin, offering valuable insights for advancing research and the development of new anticancer therapies.

ADME Properties Predictions

The SwissADME assessment of 19 metabolites derived from *R.S., C.P.*, and *C.C*. extracts determined that the majority of compounds exceeded a molecular weight of 500 Da, with the exceptions being Uzarigenin, Isorhamnetin-O-Hexoside, Apigenin-7-o-glucoside, Cirsiliol, Chlorogenic acid, Acacetin, Acetylaspidospermidine, and 15beta-Hydroxyvincadifformine. Notably, 1-Acetylaspidospermidine demonstrated the highest lipophilicity while maintaining favorable solubility, thus facilitating efficient translocation across the blood-brain barrier and ensuring high gastrointestinal absorption. Eight metabolites exhibited suboptimal to moderate aqueous solubility, yet demonstrated high gastrointestinal absorption and blood-brain barrier permeability, indicating their potential as substrates for P-glycoprotein. Four metabolites were excluded due to non-compliance with Lipinski's Rule of Five, whereas the remaining 15 metabolites emerged as promising drug candidates, potentially exhibiting reduced attrition rates during clinical trials.

CYP450 Enzymes Inhibition Profile

The concurrent use of herbal medicines and prescribed drugs poses significant safety concerns, particularly for drugs with narrow therapeutic windows.[43] Our study found that Cirsiliol and Acacetin inhibited almost all CYP groups except CYP2C19, while all *R.S*. metabolites inhibit CYP2D6. Moreover, in another study reported that Cirsiliol inhibited ATP synthesis.[44] Our findings are consistent with Zhou et al,[45] who found that Acacetin exhibited an inhibitory effect on different isoforms of CYP450, exclusively CYP1A2, CYP2B1, CYP2C11, CYP2D1, CYP2E1, and CYP3A2, indicating the significant risk of Acacetin in toxicity and drug interaction.[45] To minimize the risk of herb-drug interactions, metabolites inhibiting more than two CYP450 enzymes were excluded from further analysis. Drug metabolism in vivo is a complex process, involving not only CYP450 enzymes but also Phase I and Phase II metabolic pathways, transporters, and tissue-specific interactions. While SwissADME provides insights into potential CYP450 inhibition, it does not fully account for metabolite stability, systemic clearance, or bioavailability in physiological conditions. Therefore, further pharmacokinetic and pharmacodynamic investigations, including hepatic microsome studies and in vivo animal models, are necessary to obtain a comprehensive understanding of the metabolism and safety profile of these metabolites.

Prediction of Organ and Endpoint Toxicity Using ProTox II

ProTox-II web server analysis led to the exclusion of eight metabolites due to their toxic profiles. The remaining five metabolites showed no harmful effects and were deemed safe for human cells. Further research to optimize and enhance the oral bioavailability of the excluded compounds or explore their potential for parenteral administration may be warranted.

Prediction of Cardiotoxicity Using Pred-hERG 4.2 Online Web Server

Pred-hERG web server analysis predicted that Apigenin-7-o-glucoside, 1-Acetylaspidospermidine, and Chlorogenic acid were non-cardiotoxic with 50% confidence levels. However, Voruscharin and Uscharin were excluded due to their potential cardiotoxicity. As reported by Parhira et al,[46] Uscharin exhibited higher inhibitory effect on HIF-1 transcriptional activity than digoxin, a positive control.

Target Predictions

SWISS Target Prediction analysis identified Apigenin-7-o-glucoside, 1-Acetylaspidospermidine, and Chlorogenic acid as potential treatments for breast cancer by targeting TNF-α, Family A G protein-coupled receptor, and aldose reductase, respectively. Furthermore, Apigenin-7-o-glucoside found to have a greater cytotoxic effect by four-fold compared to apigenin against colon cancer cell line.[47] Molinspiration analysis revealed multiple targets for Apigenin-7-o-glucoside, including GPCR ligands, kinase inhibitors, nuclear inhibitors, protease inhibitors, and enzyme inhibitors. In contrast, 1-Acetylaspidospermidine and Chlorogenic acid were found to target ion channel modulators but not kinase inhibitors.

These findings provide valuable insights into the potential anticancer properties and mechanisms of action of the studied metabolites, paving the way for further investigation and development of novel cancer therapeutics.

Conclusion

This study successfully synthesized silver nanoparticles (AgNPs) using extracts from *Rhazya stricta, Calotropis procera*, and *Calligonum comosum*, demonstrating significant cytotoxic activity against multiple breast cancer cell lines and antibacterial effects against *S. aureus* and *E. coli*. The observed selectivity, with low toxicity to normal cells, highlights the potential of these plant-derived AgNPs as novel therapeutic agents. Furthermore, the identification of key metabolites like 1-Acetylaspidospermidine, Apigenin-7-o-glucoside, and Chlorogenic acid provides promising candidates for the development of safe oral anti-cancer and antibacterial drugs, warranting further investigation and optimization for future clinical applications.

Abbreviations

NPs, nanoparticles; AgNPs, silver nanoparticles; *R.S., Rhazya Stricta; C.P., Calotropis Procera; C.C., Calligonum Comosum*; ER, estrogen receptor; PR, progesterone receptor; TNBC, triple-negative breast cancer; HER2, human epidermal growth factor 2; LC-MS, liquid chromatography-mass spectrometry; KSAU-HS, king Saud bin Abdulaziz university for health sciences; $AgNO_3$, silver nitrate; TEM, transmission electron microscopy; DLS, dynamic light scattering; PDI, polydispersity index; EDS, energy-dispersive X-ray spectroscopy; FTIR, Fourier-transform infrared spectroscopy; ATR, attenuated total reflectance; ATCC, American type culture collection; DMEM, dulbecco's modified eagle medium; FBS, fetal bovine serum; EDTA, ethylenediaminetetraacetic acid; IC_{50}, half-maximal inhibitory concentration; HPLC, high-performance liquid chromatography; PTFE, polytetrafluoroethylene; LC-QTOF-MS, liquid chromatography quadrupole time-of-flight mass spectrometry; Q-TOF, quadrupole time of flight; ESI, electrospray ionization; SEM, scanning electron microscopy; SAR, structure-activity relationship; ADME, absorption, distribution, metabolism, and excretion; PASS, prediction of activity spectra for substances; CEBS, a comprehensively annotated database of toxicological data; RO5, Lipinski's Rule of Five.

Data Sharing Statement

The data presented in this study are available on request from the corresponding author.

Acknowledgments

The authors wish to convey their deepest gratitude to King Saud bin Abdulaziz University for Health Sciences for their ongoing support, as well as to the Princess Nourah bint Abdulrahman University Researchers Supporting Project (PNURSP2025R740), Riyadh, Saudi Arabia.

Funding

The authors extend their appreciation to the institutional review board at King Abdullah International Medical Research Center, Riyadh, Saudi Arabia for funding this research work through the project number: SP22R/060/05 and SP22R/047/04.

Disclosure

The authors declare that the research was conducted in the absence of any commercial or financial relationships that could be construed as a potential conflict of interest.

References

1. Fahad Ullah M. Breast cancer: current perspectives on the disease status. In: Ahmad A, editor. *Breast Cancer Metastasis and Drug Resistance*. Vol 1152. Advances in Experimental Medicine and Biology. Springer International Publishing; 2019;51–64. doi:10.1007/978-3-030-20301-6_4
2. Tsang JYS, Tse GM. Molecular classification of breast cancer. *Adv Anat Pathol*. 2020;27(1):27–35. doi:10.1097/PAP.0000000000000232
3. Pearce A, Haas M, Viney R, et al. Incidence and severity of self-reported chemotherapy side effects in routine care: a prospective cohort study. *PLoS One*. 2017;12(10):e0184360. doi:10.1371/journal.pone.0184360
4. Yesildag C, Tyushina A, Lensen M. Nano-contact transfer with gold nanoparticles on PEG hydrogels and using wrinkled PDMS-stamps. *Polymers*. 2017;9(6):199. doi:10.3390/polym9060199
5. Bukhari NA, Al-Otaibi RA, Ibhrahim MM. Phytochemical and taxonomic evaluation of Rhazya stricta in Saudi Arabia. *Saudi J Biol Sci*. 2017;24 (7):1513–1521. doi:10.1016/j.sjbs.2015.10.017
6. Alagrafi FS, Alawad AO, Abutaha NM, et al. In vitro induction of human embryonal carcinoma differentiation by a crude extract of Rhazya stricta. *BMC Complement Altern Med*. 2017;17(1):342. doi:10.1186/s12906-017-1852-7
7. Falana MB, Nurudeen QO. Evaluation of phytochemical constituents and in vitro antimicrobial activities of leaves extracts of Calotropis procera against certain human pathogens. *Not Sci Biol*. 2020;12(2):208–221. doi:10.15835/nsb12210699
8. Lantero A. Sewarine, an indole alkaloid from Rhazya stricta and a κ opioid receptor antagonist, induces apoptosis via caspase activation in various cancer cell lines, and inhibits NF-κB activation. *Intrinsic Act*. 2014;2(Suppl. 1):A1.20. doi:10.25006/IA.2.S1-A1.20
9. Nabih AB, Ayman IE, Osama AA, Mohammed HM. Potential anticancer activity of the medicinal herb, Rhazya stricta, against human breast cancer. *Afr J Biotechnol*. 2012;11(37):8960–8972. doi:10.5897/AJB12.570
10. Van Beek TA, Verpoorte R, Svendsen AB, Fokkens R. Antimicrobially active alkaloids from Tabernaemontana chippii. *J Nat Prod*. 1985;48 (3):400–423. doi:10.1021/np50039a008
11. Ali BH, Al-Qarawi AA, Bashir AK, Tanira MO. Phytochemistry, pharmacology and toxicity ofRhazya stricta Decne: a review. *Phytother Res*. 2000;14(4):229–234. doi:10.1002/1099-1573(200006)14:4<229::AID-PTR673>3.0.CO;2-5
12. Elkady AI. Crude alkaloid extract of Rhazya stricta inhibits cell growth and sensitizes human lung cancer cells to cisplatin through induction of apoptosis. *Genet Mol Biol*. 2013;36(1):12–21. doi:10.1590/S1415-47572013005000009
13. El-Awady MA, Awad NS, El-tarras AE. Evaluation of the anticancer activities of pomegranate (Punica granatum) and harmal (Rhazya stricta) plants grown in Saudi Arabia. *Int J Curr Microbiol Appl Sci*. 2015;4(5):1158–1167.
14. Abdul-Hameed ZH, Bawakid NO, Alorfi HS, et al. Monoterpene indole alkaloids from the aerial parts of Rhazya stricta induce cytotoxicity and apoptosis in human adenocarcinoma cells. *Molecules*. 2022;27(4). doi:10.3390/molecules27041422
15. Shehzad A, Qureshi M, Jabeen S, et al. Synthesis, characterization and antibacterial activity of silver nanoparticles using *Rhazya stricta*. *PeerJ*. 2018:6:e6086. doi:10.7717/peerj.6086
16. Azaizeh H, Saad B, Cooper E, Said O. Traditional Arabic and Islamic medicine, a re-emerging health aid. *Evid Based Complement Alternat Med*. 2010;7(4):419–424. doi:10.1093/ecam/nen039
17. Saad B, Azaizeh H, Said O. Tradition and perspectives of Arab herbal medicine: a review. *Evid Based Complement Alternat Med*. 2005;2(4):475–479. doi:10.1093/ecam/neh133
18. Alzahrani AJ. Potent antioxidant and anticancer activities of the methanolic extract of Calligonum comosum (L'Her) fruit hairs against human hepatocarcinoma cells. *Saudi J Biol Sci*. 2021;28(9):5283–5289. doi:10.1016/j.sjbs.2021.05.053
19. Badria FA, Ameen M, Akl MR. Evaluation of cytotoxic compounds from Calligonum comosum L. Growing in Egypt. *Z Für Naturforschung C*. 2007;62(9–10):656–660. doi:10.1515/znc-2007-9-1005
20. Ali R, Al Zahrani H, Barhoumi T, et al. Isolation and establishment of a highly proliferative, cancer stem cell-like, and naturally immortalized triple-negative breast cancer cell line, KAIMRC2. *Cells*. 2021;10(6):1303. doi:10.3390/cells10061303
21. Alghamdi SS, Alturki AY, Ali R, et al. Pharmacological profiling of Calotropis procera and Rhazya stricta: unraveling the antibacterial and anti-cancer potential of chemically active metabolites. *J Cancer*. 2025;16(1):12–33. doi:10.7150/jca.96848
22. Lagunin A, Stepanchikova A, Filimonov D, Poroikov V. PASS: prediction of activity spectra for biologically active substances. *Bioinformatics*. 2000;16(8):747–748. doi:10.1093/bioinformatics/16.8.747
23. Daina A, Michielin O, Zoete V. SwissADME: a free web tool to evaluate pharmacokinetics, drug-likeness and medicinal chemistry friendliness of small molecules. *Sci Rep*. 2017;7(1):42717. doi:10.1038/srep42717
24. Banerjee P, Eckert AO, Schrey AK, Preissner R. ProTox-II: a webserver for the prediction of toxicity of chemicals. *Nucleic Acids Res*. 2018;46 (W1):W257–W263. doi:10.1093/nar/gky318
25. Braga RC, Alves VM, Silva MFB, et al. Pred-hERG: a novel web-accessible computational tool for predicting cardiac toxicity. *Mol Inform*. 2015;34(10):698–701. doi:10.1002/minf.201500040
26. Hadda TB, Rastija V, AlMalki F, et al. Petra/Osiris/Molinspiration and molecular docking analyses of 3-hydroxy-indolin-2-one derivatives as potential antiviral agents. *Curr Comput Aided Drug Des*. 2021;17(1):123–133. doi:10.2174/1573409916666191226110029
27. Gfeller D, Grosdidier A, Wirth M, Daina A, Michielin O, Zoete V. SwissTargetPrediction: a web server for target prediction of bioactive small molecules. *Nucleic Acids Res*. 2014;42(Web Server issue):W32–38. doi:10.1093/nar/gku293
28. Daina A, Michielin O, Zoete V. SwissTargetPrediction: updated data and new features for efficient prediction of protein targets of small molecules. *Nucleic Acids Res*. 2019;47(W1):W357–W364. doi:10.1093/nar/gkz382
29. Shinde A, Jung H, Lee H, et al. TNF-α differentially modulates subunit levels of respiratory electron transport complexes of ER/PR +ve/−ve breast cancer cells to regulate mitochondrial complex activity and tumorigenic potential. *Cancer Metab*. 2021;9(1):19. doi:10.1186/s40170-021-00254-9
30. Singh A, Nunes JJ, Ateeq B. Role and therapeutic potential of G-protein coupled receptors in breast cancer progression and metastases. *Eur J Pharmacol*. 2015;763(Pt B):178–183. doi:10.1016/j.ejphar.2015.05.011

31. Singh M, Kapoor A, Bhatnagar A. Physiological and pathological roles of aldose reductase. *Metabolites*. 2021;11(10). doi:10.3390/metabo11100655
32. Batool A, Menaa F, Uzair B, Khan BA, Menaa B. Progress and prospects in translating nanobiotechnology in medical theranostics. *Curr Nanosci*. 2020;16(5):685–707. doi:10.2174/1573413715666191126093258
33. Mohanta YK, Biswas K, Jena SK, Hashem A, Abd_Allah EF, Mohanta TK. Anti-biofilm and antibacterial activities of silver nanoparticles synthesized by the reducing activity of phytoconstituents present in the Indian medicinal plants. *Front Microbiol*. 2020;11:1143. doi:10.3389/fmicb.2020.01143
34. Vijilvani C, Bindhu MR, Frincy FC, et al. Antimicrobial and catalytic activities of biosynthesized gold, silver and palladium nanoparticles from Solanum nigurum leaves. *J Photochem Photobiol B*. 2020;202:111713. doi:10.1016/j.jphotobiol.2019.111713
35. Mittal AK, Chisti Y, Banerjee UC. Synthesis of metallic nanoparticles using plant extracts. *Biotechnol Adv*. 2013;31(2):346–356. doi:10.1016/j.biotechadv.2013.01.003
36. Rahman H, Rauf A, Khan SA, et al. Green synthesis of silver nanoparticles using Rhazya stricta Decne extracts and their anti-microbial and anti-oxidant activities. *Crystals*. 2023;13(3):398. doi:10.3390/cryst13030398
37. Al-Sahli SA, Al-Otibi F, Alharbi RI, Amina M, Al Musayeib NM. Silver nanoparticles improve the fungicidal properties of Rhazya stricta decne aqueous extract against plant pathogens. *Sci Rep*. 2024;14(1):1297. doi:10.1038/s41598-024-51855-5
38. Chandhru M, Logesh R, Kutti Rani S, Ahmed N, Vasimalai N. Green synthesis of silver nanoparticles from plant latex and their antibacterial and photocatalytic studies. *Environ Technol*. 2022;43(20):3064–3074. doi:10.1080/09593330.2021.1914181
39. Alghamdi SS, Alshafi RA, Huwaizi S, et al. Exploring in vitro and in silico biological activities of Calligonum comosum and Rumex vesicarius: implications on anticancer and antibacterial therapeutics. *Saudi Pharm J*. 2023;31(11):101794. doi:10.1016/j.jsps.2023.101794
40. Sagadevan S, Vennila S, Muthukrishnan L, et al. Exploring the therapeutic potentials of phyto-mediated silver nanoparticles formed via *Calotropis procera* (Ait.) R. Br. root extract. *J Exp Nanosci*. 2020;15(1):217–231. doi:10.1080/17458080.2020.1769842
41. Algebaly AS, Mohammed AE, Abutaha N, Elobeid MM. Biogenic synthesis of silver nanoparticles: antibacterial and cytotoxic potential. *Saudi J Biol Sci*. 2020;27(5):1340–1351. doi:10.1016/j.sjbs.2019.12.014
42. Wadhwani BD, Mali D, Vyas P, Nair R, Khandelwal P. A review on phytochemical constituents and pharmacological potential of *Calotropis procera*. *RSC Adv*. 2021;11(57):35854–35878. doi:10.1039/D1RA06703F
43. Chen XW, Sneed KB, Pan SY, et al. Herb-drug interactions and mechanistic and clinical considerations. *Curr Drug Metab*. 2012;13(5):640–651. doi:10.2174/1389200211209050640
44. Carlini L, Tancreda G, Iobbi V, et al. The flavone Cirsiliol from Salvia x jamensis binds the F1 moiety of ATP synthase, modulating free radical production. *Cells*. 2022;11(19):3169. doi:10.3390/cells11193169
45. Zhou Y, Tu Y, Zhou Q, et al. Evaluation of acacetin inhibition potential against cytochrome P450 in vitro and in vivo. *Chem Biol Interact*. 2020;329:109147. doi:10.1016/j.cbi.2020.109147
46. Parhira S, Zhu GY, Jiang RW, Liu L, Bai LP, Jiang ZH. 2'-Epi-uscharin from the latex of Calotropis gigantea with HIF-1 inhibitory activity. *Sci Rep*. 2014;4:4748. doi:10.1038/srep04748
47. Smiljkovic M, Stanisavljevic D, Stojkovic D, et al. Apigenin-7-O-glucoside versus apigenin: insight into the modes of anticandidal and cytotoxic actions. *EXCLI J*. 2017;16:795–807. doi:10.17179/excli2017-300